Sādhanā, Vol. 14, Part 3, December 1989, pp. 133–172. © Printed in India.

Cellular automaton fluids – A review

M RAJ LAKSHMI

Centre for Atmospheric Sciences, Indian Institute of Science, Bangalore 560012, India

MS received 3 April 1989

Abstract. This paper is basically a review of cellular automaton fluids, which are the class of cellular automata used for describing fluids. Cellular automaton fluids are discrete analogues of molecular dynamics in which the particles have discrete velocities and move on the sites of a lattice according to some rule of evolution. We restrict ourselves mainly to two-dimensional fluids, but make some comments regarding models for fluids in three dimensions. Analytical as well as numerical simulation results, including ours on the wake behind a cylinder, are discussed for the two-dimensional cellular automaton (CA) models. We also discuss briefly some issues which need resolution before the CA models can be used for practical simulations.

Keywords. Cellular automata; two-dimensional fluids; cellular automaton fluids.

1. Introduction

In recent years there has been a great deal of interest in the field of cellular automata in general (Wolfram 1986a). Of interest to us here is a sub-field, namely cellular automaton fluids, which as the name suggests, are models that are used for the simulation of fluid dynamics. Though a relatively new area, a lot of research has been done in modelling fluids using cellular automata (CA), mostly in the last two years. The great interest stems from the hope that the CA models will provide an ideal simulation strategy for fluid dynamics. This paper is basically a review of the subject of CA fluids. It is by no means exhaustive; rather, we have concentrated on discussing some of the issues in reasonable depth.

A cellular automaton is a fully discrete dynamical system. It is constituted of a lattice, with each site (vertex) having a finite number of discrete states. The automaton evolves in time in discrete steps, and the dynamics is specified by some given rule, which may be deterministic or non-deterministic (probabilistic). CA were introduced as long back as in 1963 (von Neumann 1963, p. 288, 1966) however, only in the last few years has there been renewed interest in them, and this is largely because of the general availability of computers with massively parallel architectures.

Even though CA are discrete in nature, if sufficiently large, they can show continuous macroscopic behaviour. That is, CA are capable of modelling continuum systems such

as fluids. We shall refer to this class of CA as "CA fluids" or "CA lattice-gas models". We will be concerned only with those lattice-gas models that lead to the Navier–Stokes equations. Historically, they emerged from attempts to construct discrete models of fluids with varying motivations. The aim of molecular dynamics (see, for example, Boon & Yip 1980) is to simulate the real microworld by considering the system of discrete particles with continuous time, positions and velocities, and arbitrary interactions. In the discrete velocity models introduced by Broadwell, the velocity set is finite, but space and time are still continuous and the evolution is probabilistic (Broadwell 1964). The first lattice-gas model (referred to as the HPP model) with discrete time, positions and velocities and deterministic evolution, was introduced by Hardy *et al* (1973, 1976; see also Hardy & Pomeau 1972). Their motivation was to analyse, both numerically and analytically, fundamental questions in statistical mechanics, such as ergodicity and the divergence of transport coefficients in two dimensions in as simple a framework as possible. However, the HPP model suffered from various drawbacks and was not able to reproduce the full fluid dynamical behaviour. These difficulties were overcome several years later by Frisch *et al* (1986) for the two-dimensional Navier–Stokes (NS) equation. Their model is commonly referred to as the FHP model. Since then, there has been a burgeoning of interest and activity in this field (for references, see Frisch *et al* 1987). Some analytical results have been obtained and several numerical simulations have been performed. It has been shown (Wolfram 1986; Rivet & Frisch 1986), using methods from kinetic theory, that (under certain conditions) the macroscopic behaviour of the FHP cellular automaton model corresponds to the standard incompressible Navier–Stokes equations, in two dimensions, for fluid flow. Qualitative, and in some cases quantitative, agreement between theory and simulation has been demonstrated in both the linear and nonlinear regimes (Hayot & Raj Lakshmi 1989; for other references, see d'Humieres & Lallemand 1987). Expected hydrodynamical behaviour has been reproduced.

Several variants of the basic FHP model for fluids in two dimensions have been written down. These differ from the original model in that they allow for either a different number of possible states at each site or a different rule of evolution or a combination of both. All of them lead to the same macrodynamical equation, namely the Navier–Stokes equation, but transport coefficients such as the viscosity have different values in the various models. This is because the form of the macroscopic equations is entirely governed by the microscopic conservation laws and symmetries, whereas the transport coefficients depend on the details of the microphysics.

However, for the more realistic, and practically more useful, case of three dimensions, the situation is not yet fully clear. Some models have been introduced very recently to describe fluids in three dimensions (d'Humieres *et al* 1986), but none of them is very efficient. There are several other important and interesting open questions too; for example, the proper incorporation of thermal effects and ways to overcome the "practical limitations" arguments of Orszag & Yakhot (1986), to name only a few.

The rest of the paper is organized as follows. In the next section, §2, we give a brief history of cellular automata in general. Thereafter, starting from §3, we concentrate on the CA models for fluids, and in particular on models leading to the Navier–Stokes equations. In §3 we discuss the first fully discrete model, the HPP model for describing fluids in two dimensions. The drawbacks of this model in leading to the two-dimensional Navier–Stokes equation are also given. The FHP model, which overcomes these difficulties, is introduced in §4. In this section, we describe the FHP model in detail and we also give a summary of the analytical results for this model. The

computer simulations on the basic FHP model and its variants are described briefly in §5. We also present our results for the simulations of the wake of a cylinder in two dimensions. The details of the derivation of the Navier–Stokes equations for the FHP model are given in §6; as already mentioned the results and the outline of the derivation are covered in §4. Section 7 deals with some open problems, such as models for fluids in three dimensions and thermal effects; it includes some of our ideas for incorporating thermal effects properly. In this section, we also present the arguments of Orszag & Yakhot (1986) for their reservations about CA models being a viable alternative to conventional simulations of the Navier–Stokes equations, especially at high Reynolds numbers. We end the paper and the section with some concluding remarks.

2. Brief history of cellular automata

The best known and illustrative example of a cellular automaton is John H Conway's *Game of Life* (Gardner 1970). This game describes the multiplication and extinction in a population of "cells" or a society of organisms and is a two-dimensional cellular automaton (CA).

One starts with a two-dimensional square lattice, in which each cell is either "live" (denoted by a '1') or "dead" (denoted by a '0'). In each 3×3 region, therefore, there is a centre cell and 8 adjacent cells. These 8 cells form the neighbourhood (Moore neighbours) of the centre cell. The new state of each cell is determined by the rule of "Life". This rule states that, at the next generation, a live cell remains live iff it has 2 or 3 live neighbours; otherwise, it dies (either by "isolation" or "over-crowding"). A dead cell revives, i.e., becomes live, iff it has 3 live neighbours; otherwise, it stays dead. Figure 1 illustrates this rule.

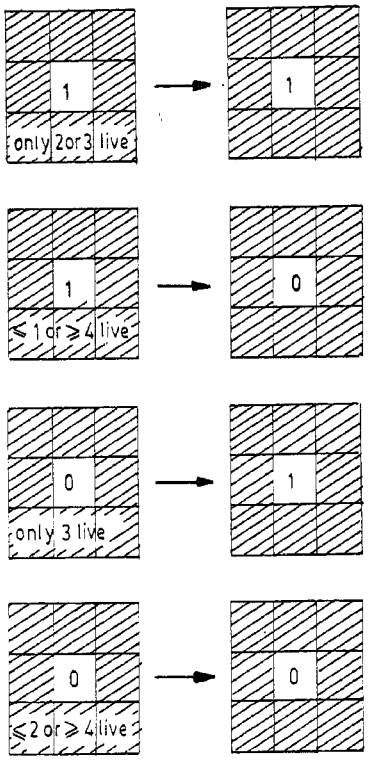

Figure 1. Illustrates the rule of evolution in the "Game of Life". The shaded region consisting of eight cells forms the neighbourhood of the centre cell and determines its state at the next time step. A '1' or a '0' in the cell denotes that it is "live" or "dead", respectively.

When one starts with various initial configurations and lets them evolve according to the rule mentioned, one finds several remarkable features: (i) simple rules can give complex behaviour, (ii) ordered patterns out of disordered ones ("primeval soup"), (iii) the eventual fate of simple initial patterns is either "death" (i.e., the patterns become all zeros), or "still life" (unchanging with time) or "oscillations" (i.e., a cycle of configurations that keeps repeating), and (iv) slightly different initial patterns have widely different final fates. Results for some sample starting configurations are shown in figure 2, which has been taken from Martin Gardner's article (Gardner 1970). These figures illustrate some of the features discussed just now.

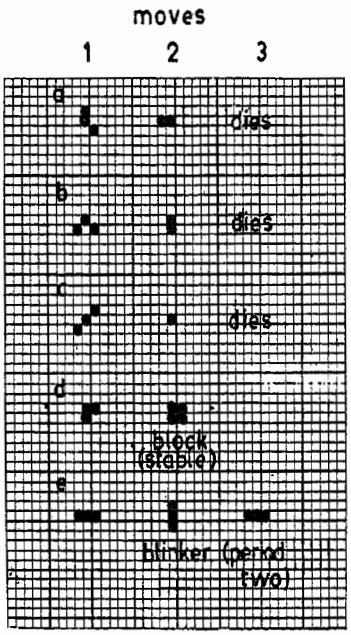

(2A)

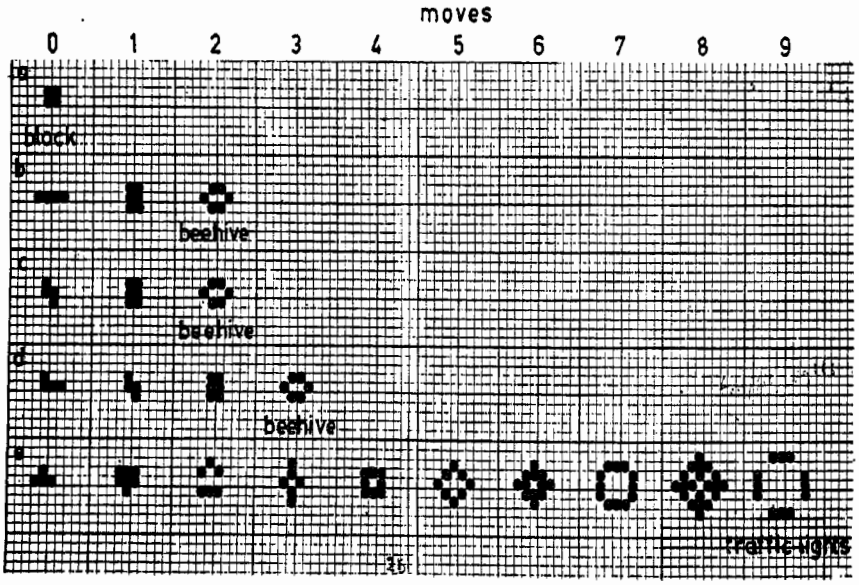

(2B)

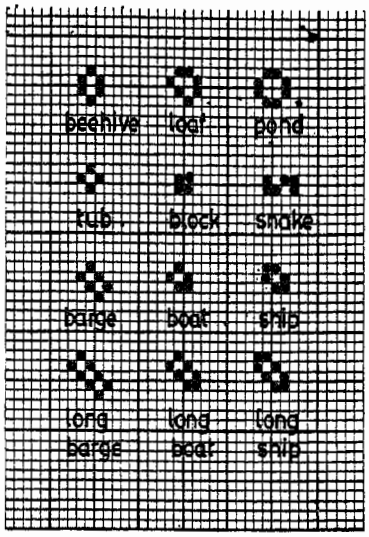

(2C)

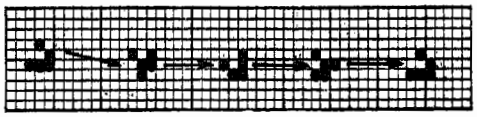

(2D)

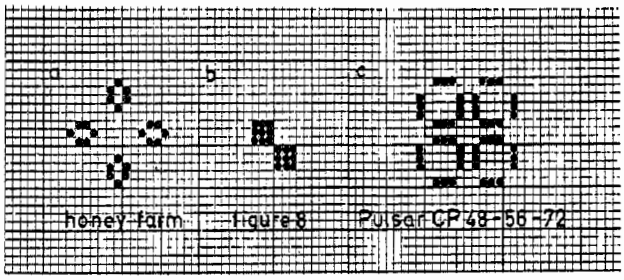

(2E)

Figure 2. Fates of certain simple starting configurations in the "Game of Life" (taken from Gardner 1970). (**A**) The fate of five triplets in "life". (**B**) The life histories of the five tetrominoes. (**C**) The commonest stable forms (**D**) The "glider", (**E**) Three remarkable patterns, one stable and two oscillating.

Now we can abstract this game and answer the question: "What is a cellular automaton?" It is a fully discrete dynamical system (in any dimension) with the following basic characteristics:

(a) it is discrete in space,
(b) it is discrete in time,
(c) it has discrete states,
(d) the rule of evolution is fixed and definite. This rule, in general, has many simplifying features; it

(i) is homogeneous (or uniform) – all cells evolve by the same rule (inhomogeneous CA have been considered too);
(ii) allows for synchronous updating – all cells can be updated simultaneously;

(iii) is deterministic – the rules don't have any randomness in them; (probabilistic CA have also been studied, where the rules are applied at each cell and at each time step probabilistically);
(iv) is spatially local – the rule depends only on a small neighbourhood;
(v) is temporally local – the rule depends only on cell values at the previous time-step, or a few previous ones.

For example, the rule of evolution for the "Game of Life" has all the above simplifying features – the rule can be written as:

$$c_{ij}^{t+1} = f(c_{i-1j-1}^{t}, c_{i-1j}^{t}, c_{i-1j+1}^{t}, c_{ij+1}^{t}, c_{i+1j+1}^{t}, c_{i+1j}^{t}, c_{i+1j-1}^{t}, c_{ij-1}^{t}),$$

where c_{ij}^{t} is the state of the (i, j)th cell at time t, and the function f is

$$f(2 \text{ "live" neighbours}) = c_{ij}^{t}$$
$$f(3 \text{ "live" neighbours}) = 1$$
$$f(\text{all other cases}) = 0.$$

With these characteristics, CA provide rather general discrete models for homogeneous models with local interactions. Though each cell is discrete, collections of cells can show effectively continuous behaviour.

Cellular automata were introduced as early as in 1963 by von Neumann and Ulam (under the name "cellular spaces") to "abstract the logical structure of life" (von Neumann 1963). They were used as a possible idealization of biological systems, with the purpose of modelling biological self-reproduction. Since then, many biological systems have been modelled by CA with a view to studying the development of structure and patterns in the growth, behaviour and functioning of organisms, populations of non-mobile organisms etc.

CA have come under several other names too: tesselation automata, homogeneous structures, cellular structures, iterative arrays, to name but a few.

In fact, computational systems (i.e., computers) can essentially be viewed as cellular automata. The processing of data (given as initial conditions) is done according to some rule of evolution, given by the computer program. Here, of course, several conditions on the rule are relaxed, in particular, the condition that the rule be homogeneous in space and time. However, if the rules (as specified earlier in this section) are strictly obeyed (especially the simplifying features of synchronous updating, homogeneity and locality), then cellular automata can be used as general paradigms for parallel computation (cf. Manning 1977; Preston *et al* 1979). Also, some CA are capable of universal computation (for references, see Wolfram 1984). A universal computer is one in which changes in input alone allow any "computable function" to be evaluated, without any change in internal construction. It has been shown that the game-of-life CA is computationally universal. This is discussed by Wolfram (1983, 1984).

There have been several applications of CA to physical systems too. Physical systems which contain many discrete elements with local interactions can often be conveniently modelled as CA. Nontrivial CA are obtained whenever the dependence on the values at each site is nonlinear. A very wide variety of examples of CA applications exists; only a few are mentioned here. Nonlinear chemical systems involving a network of reactions coupled with spatial diffusion have been modelled using CA (Greenberg *et al* 1978), as also the growth of dendritic crystals (Langer 1980). In the latter, probabilistic CA are used. The dynamical Ising model (cf. Kawasaki 1972) (i.e., with

the kinetic energy terms included) and other lattice spin systems are examples of CA. These CA are also non-deterministic (i.e., probabilistic) because of "noise" in the local rules at finite temperature. In all these cases, the CA lattice is in position space. Cellular automata in momentum space, with site values representing excitations of the corresponding modes, also describe physical systems.

CA have also been used to study problems in number theory (Sutton 1981), and extensively for image processing and visual pattern recognition especially in two dimensions (Rosenfeld 1979; Sternberg 1980).

3. The HPP model for fluids in two dimensions

In the context of fluid mechanics, Hardy *et al* (1973) proposed a model (the HPP model) to study the dynamics of a fully discrete two-dimensional system of interacting classical particles. (Related models with discrete sets of velocities but with continuous space–time were introduced by Broadwell 1964). Their motivation was to study properties like ergodicity, mixing, approach to equilibrium etc. in a model system (as simple as possible) where some exact calculations could be performed, and simulations of which are exact (Hardy *et al* 1973, 1976; Hardy & Pomeau 1972). They also wanted to check various theoretical predictions of the asymptotic behaviour of time correlation functions in classical two-dimensional fluids. The hope was, though denied in their paper, that this model would play the same role for fluids as the Ising model does for equilibrium statistical mechanics.

The HPP model lives on a regular, square, two-dimensional lattice with unit edge (link) lengths. Particles (of unit mass) sit at lattice sites, have unit speed, and velocities pointing along one of the four link directions. An exclusion rule is imposed whereby no two (or more) particles at any site can have velocities pointing in the same direction, at any time. This implies that the maximum occupation is 4 particles per site. A sample configuration on a small portion of the HPP lattice is shown in figure 3a.

The rule of evolution for the configurations is deterministic, and consists of two steps, translation and collision, in unit time.

(i) *Translation step* – Each particle is allowed to travel for unit time, with its own velocity. This is equivalent to moving the particle by one link, to the nearest site to which its velocity is pointing. Figure 3b shows the results of performing this operation on the configuration of figure 3a.

(ii) *Collision step* – In this, particles at each site are rearranged according to some prescribed collision rules. In the HPP model, only 2-particle head-on collisions (zero impact parameter) are allowed, in which the two particles change their directions by 90°. All other configurations are unchanged. Figure 3c shows the resulting configuration at the end of one time step.

It is clear that the rule of evolution conserves particle number and momentum. Energy is then automatically conserved since each particle has the same kinetic energy, and the number of particles does not change.

This completes the description of the model. The underlying lattice and the type of particles residing on it have been specified. Given any initial configuration, the rule of evolution determines uniquely the configuration at any later time.

We shall now state some of the results for the HPP model. It has been shown by Hardy *et al* (1972, 1973, 1976) that thermodynamic equilibrium exists for this model.

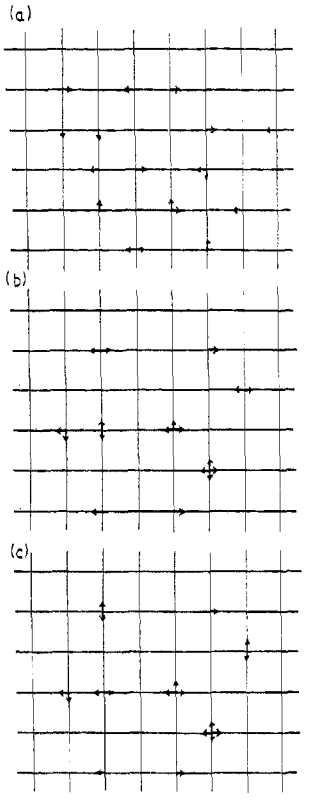

Figure 3. Successive configurations in the HPP lattice-gas model illustrating the rules. Each arrow represents a particle at a lattice site with velocity pointing along the direction of the arrow. Configurations are shown in (**a**) at some time t; (**b**) after the action of the translation step on (a); (**c**) after the action of the collision step on (b); this is the final configuration at time $(t+1)$.

Properties such as relaxation and transport have been investigated using conventional approaches. Relaxation to equilibrium has been demonstrated numerically. However, pathologies were found in the transport properties. This is essentially due to the effective one-dimensional behaviour, even though the underlying lattice is two-dimensional. This in turn is due to the extra conservation law present in the model – momentum is conserved separately on each row and column! This can, however, be remedied quite easily, but we will not go into the details here (see Margolus *et al* 1986).

Nevertheless, numerical simulations did not reproduce the macroscopic behaviour correctly. In fact, the "macrodynamical" equations derived from this model differ from the Navier–Stokes equations [in §2(d)] in two major respects:

(i) *Lack of Galilean invariance* – Galilean invariance means that the governing equations must be invariant under a Galilean transformation, i.e., under the transformation

$$x' = x + Ut, \quad t' = t, \tag{1}$$

where primes denote quantities in the new frame of reference, moving with an arbitrary, uniform velocity $\mathbf{u}$ with respect to the original frame. (It is easy to check that the Navier–Stokes (NS) equations are Galilean invariant). But the equations for the HPP model are not. The momentum flux tensor here is found to be

$$\pi_{\alpha\beta} = p\delta_{\alpha\beta} + T_{\alpha\beta\gamma\varepsilon}u_\gamma u_\varepsilon + O(u^4), \tag{2}$$

where **u** is the macroscopic (coarse-grained) velocity. The terms of $O(u^4)$ and higher, break Galilean invariance. However, this problem can be overcome by restricting to low Mach numbers, whence these terms will be negligible.

(ii) *Lack of isotropy* – For the HPP model, it can be shown (this will be outlined later) that the tensor $T_{\alpha\beta\gamma\varepsilon}$ is not isotropic. Hence the quadratic term in $\pi_{\alpha\beta}$ will not be of the form $\rho u_\alpha u_\beta$ and therefore the quadratic (convective) term in the NS equation cannot be obtained. This is a serious problem and is due to insufficient symmetry at the level of the lattice.

It is therefore not surprising that interest in the HPP model and in the totally discrete approach to fluids, waned.

4. The FHP model for fluids in two dimensions

In the last three years, however, there has been a great revival of interest in cellular automaton models for fluids. This is due to the work of Frisch, Hasslacher & Pomeau (FHP) who proposed a slightly different CA lattice gas model for two-dimensional fluids, which overcomes the isotropy problem (Frisch *et al* 1986). This model (hereafter called the FHP model) is actually very similar to the HPP model discussed in the previous section.

4.1 *Description of the FHP model*

The FHP model lives on a triangular lattice in two dimensions (i.e., the space is covered by hexagonal cells). In fact, this is the main difference between the two models; the symmetry of the lattice is higher now. All links on the lattice have the same length, equal to unity.

All the particles reside at lattice sites (/nodes/vertices), have unit mass and unit speed but with velocities along one of the six directions, shown in figure 4. Therefore, all particles have the same kinetic energy. In this model too, an exclusion principle is used, which restricts to one, the number of particles with a particular velocity-direction that can reside at any site (at any time). This then implies that there can only be a maximum of 6 particles at a site. A 'snapshot' picture of a sample configuration at some time t is shown in figure 5.

As before, the rule of evolution which gives the configuration at time $t+1$, and hence at any later time, consists of (for each time step) a translation step and a collision step. In the translation step, the particles travel to their neighbouring sites, in the direction of their velocity (this is the distance that unit speed particles cover in unit time).

In the collision step, there is a rearrangement of the particles at each site according to a definite set of rules, which conserve particle number and momentum. (As before, energy conservation is not independent, but is automatically satisfied). The rules for

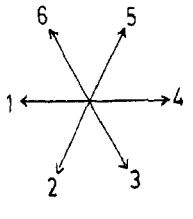

Figure 4. Shows the six directions for the particle velocities in the FHP model.

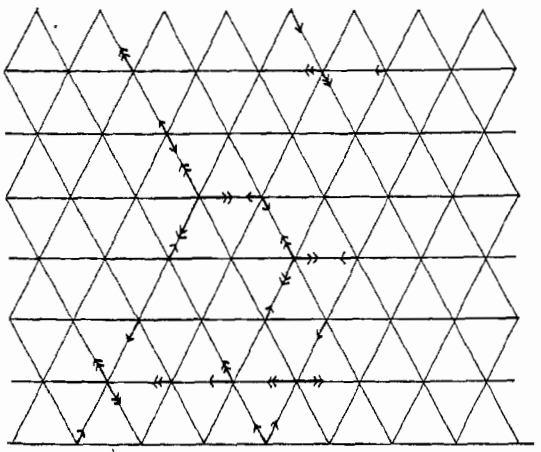

Figure 5. Typical configurations in the FHP lattice gas model I. Particles at time t and $(t+1)$ are shown by single and double arrows respectively.

the original FHP model allow only 2-particle and symmetric 3-particle collisions. In the 2-particle collision, two particles colliding head-on reorient by $\pm 60°$ as shown in figure 6a. In the symmetric 3-particle collision (shown below), the configuration of three particles with velocities along alternate links, is rotated by 60°. This is shown in figure 6b. All other configurations remain unchanged.

With these rules, one gets the correct number of local conservation laws – one for particle number and two for momentum (a two-dimensional vector). In fact, 3-particle collisions are essential to avoid spurious conservation laws. It is not difficult to see that with only 2-particle collisions, there is an extra conservation law, i.e., four (instead of three) scalar quantities are independently conserved. These are given by $(n_1+n_2+n_3+n_4+n_5+n_6)$, (n_1-n_4), (n_2-n_5) and (n_3-n_6) where n_i is the number of particles ($=0$ or 1) at a site with velocity along the ith direction (see figure 4). These scalars are nothing but the particle number and momenta along the three directions.

These rules also safeguard the exclusion rule, so that, if the initial configuration is chosen to satisfy the exclusion principle, then the configuration at any later time (obtained using the rule of evolution) will definitely have the same property. Further, if the rule for 2-particle collisions is used as a deterministic rule (for example, by specifying a priori which of the two outcomes will hold at any particular site on the lattice), then the CA model will obey microscopic reversibility. This is because each configuration has a unique successor and a unique predecessor.

4.1a *Boundary conditions*: These are very easy to implement in any CA lattice-gas model. The conditions which are normally used are the following: at obstacles/fixed boundaries, either a "bounce-back", or "specular" reflection through 120° or a

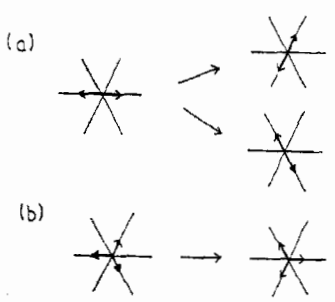

Figure 6. Schematic representation of allowed collisions in the FHP model 1, (**a**) shows 2-particle collisions, and (**b**) shows the 3-particle collision (this is a symmetric collision and is the only one allowed).

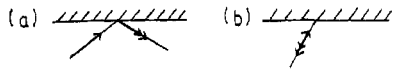

Figure 7. Conditions at fixed boundaries/obstacles. (**a**) shows the "specular reflection" condition, and (**b**) shows the "bounce-back" condition.

combination of the two conditions can be used. In the "bounce-back" condition, when the particles hit the boundary, their velocities get reversed (i.e., $\mathbf{v} \rightarrow -\mathbf{v}$); this yields "no slip" on average. In the latter condition, particles are specularly reflected through 120°; this gives "free-slip". Both conditions are illustrated in figure 7.

At lattice boundaries, one can use either periodic conditions in one or both directions, or a "wind-tunnel" type condition. In the latter, particles are generated and absorbed at lattice edges up- and downstream.

4.1b *Modifications of the basic FHP model*: The original FHP model (we will refer to it as model I) is almost the simplest one that has the minimal features necessary to reproduce correctly the macroscopic behaviour of two-dimensional classical fluids. One can write down several more elaborate versions of the same basic model, for example, by including more collisions or by allowing more particles per site etc. These modifications do not really affect the form of the macroscopic equations corresponding to the models. But they are important in determining parameters such as the viscosity etc., as will be clear later. We only give some of the modified models studied so far (see, d'Humieres & Lallemand 1986):

(i) the same 6-particles/site model but with more collisions included, e.g., asymmetric 3-particle collisions, 4-particle collisions etc. Figure 8 gives all possible collisions for such a model that still conserve particle number and momentum.
(ii) a 7-particles/site model, in which an extra particle with speed zero is allowed at each site (model II). This particle is assumed to have internal energy so as to allow for energy conservation during collisions. The additional collisions allowed in model II, besides those in the original model I, are shown in figure 9.
(iii) the same 7-particles/site model (i.e., with one rest particle) but with all possible collisions, permissible by conservation relations, allowed. We shall refer to this as model III.

4.2 *Summary of analytical results for the FHP model*

For any such cellular automaton model, the macroscopic variations of conserved quantities such as particle number and momentum can be described by continuum

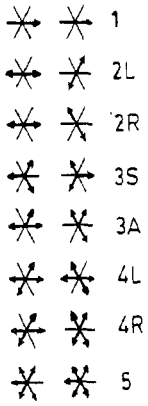

Figure 8. All possible types (classes) of initial and final states for collisions in the FHP lattice-gas model.

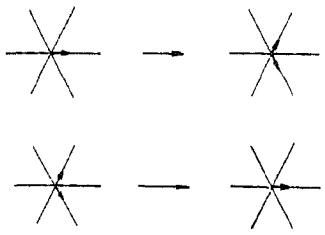

Figure 9. Additional collision rules (beyond those shown in figure 6) for model II which has rest particles.

equations. Some of these models (such as the FHP model and its variants) yield exactly the usual 2-D incompressible NS equations for hydrodynamics, to some order in a particular expansion (Frisch *et al* 1986; Wolfram 1986; Rivet & Frisch 1986). We shall summarize the results for the FHP model here, and give the details of derivation in §6. For the most part, we will describe the original FHP model (model I); differences for models II and III will also be pointed out.

We need to define some notation first. Let the six links out of each site be denoted by $\hat{e}_1, \hat{e}_2, \hat{e}_3, \hat{e}_4, \hat{e}_5, \hat{e}_6$ where

$$\hat{e}_a = [\cos(2\pi a/6), \sin(2\pi a/6)] \tag{3}$$

is a vector in two dimensions. In model I, all particles have unit velocity, given by $\hat{e}_a$ with some a ($a = 1, 2, \ldots, 6$). As in the case of conventional gases, here too we work with the one-particle distribution function, denoted here by $f_a(\mathbf{x}, t)$, which gives the probability of finding a particle with velocity $\hat{e}_a$ at position $\mathbf{x}$ and time t. [This quantity is the analog of the function $f(\mathbf{v}, \mathbf{x}, t)$ in conventional gases].

The master equation for $f_a(\mathbf{x}, t)$ is

$$\partial_t f_a + \hat{e}_a \cdot \nabla f_a = \Omega_a. \tag{4}$$

Here, Ω_a is the collision term (assumed to be local). The above equation is nothing but the conventional Boltzmann equation with the full collision term. Corrections to the above equation due to the discreteness of space and time can easily be written down. Macroscopic average quantities, such as the particle density ρ and the momentum density $\rho\mathbf{u}$ are determined in terms of f_a by:

$$\rho = \sum_a f_a; \quad \rho\mathbf{u} = \sum_a \hat{e}_a f_a. \tag{5}$$

(In the case of normal fluids (cf. Huang 1965), these two quantities are nothing but $\rho(\mathbf{x}, t) = \int d\mathbf{v} f(\mathbf{v}, \mathbf{x}, t)$ and $\rho\mathbf{u} = \int d\mathbf{v} \mathbf{v} f(\mathbf{v}, \mathbf{x}, t)$). The details of the collisions, represented by the term Ω_a, are irrelevant for determining the form of the macroscopic equations; they only affect the transport coefficients.

The hydrodynamic equations for ρ and $\rho\mathbf{u}$ are obtained as below.

$$\partial_t \rho + \nabla \cdot (\rho\mathbf{u}) = 0, \tag{6a}$$

$$\partial_t(\rho\mathbf{u}) + \tfrac{1}{4}\rho c^{(2)}\{(\mathbf{u}\cdot\nabla)\mathbf{u} + [\mathbf{u}(\nabla\cdot\mathbf{u}) - \tfrac{1}{2}\nabla|u|^2]\}$$
$$= -\tfrac{1}{2}\nabla\rho - \tfrac{1}{8}\rho c_V^{(2)}\nabla^2\mathbf{u} - \tfrac{1}{4}\Theta, \tag{6b}$$

where

$$\Theta = \mathbf{u}(\mathbf{u}\cdot\nabla)(\rho c^{(2)}) - \tfrac{1}{2}|u|^2\nabla(\rho c^{(2)}) + (\mathbf{u}\cdot\nabla)(\rho c_V^{(2)}) - \tfrac{1}{2}(\nabla\cdot\mathbf{u})\nabla(\rho c_V^{(2)}).$$

The quantities $c^{(2)}$ and $c_\nabla^{(2)}$ are functions of ρ and are the coefficients of a Chapman–Enskog expansion of f_a in powers of the velocity $\mathbf{u}$ and its gradient,

$$f_a = f\{1 + c^{(1)}\hat{e}_a\cdot\mathbf{u} + c^{(2)}[(\hat{e}_a\cdot\mathbf{u})^2 - \tfrac{1}{2}|\mathbf{u}|^2] + c_\nabla^{(2)}[(\hat{e}_a\cdot\nabla)(\hat{e}_a\cdot\mathbf{u}) - \tfrac{1}{2}\nabla\cdot\mathbf{u}] + \cdots\}. \tag{7}$$

The coefficients $c^{(1)}$ and $c^{(2)}$ of the non-derivative terms can be obtained from the (local) equilibrium distribution function (with a non-zero macroscopic velocity $\mathbf{u}$)

$$f_a^{eq} = \{1 + \exp[\alpha + \beta\mathbf{u}\cdot\hat{e}_a]\}^{-1}. \tag{8}$$

Compare this with the corresponding Maxwell–Boltzmann (MB) distribution function

$$f_{MB} = \exp[-\alpha - \beta m v^2/2 - \gamma\mathbf{v}\cdot\mathbf{u}]. \tag{9}$$

No specific form for Ω_a is needed. For model I, these coefficients are found to be

$$c^{(1)} = 2; \quad c^{(2)} = 2(1-2f)/(1-f) \equiv 4(\rho-3)/(\rho-6). \tag{10}$$

In deriving some of the terms of (6b), the incompressible limit has been used. Consistent with this then, the term containing $\mathbf{u}(\nabla\cdot\mathbf{u})$ can be dropped. A weaker condition, viz. that $u^2\nabla\rho$ is small, is sufficient to neglect the terms collectively denoted by Θ. Thus, for low velocities (i.e., low Mach numbers) and low gradients (usual condition for hydrodynamic processes), (6b) is nothing but the usual Navier–Stokes equation in two dimensions:

$$\partial_t(\rho\mathbf{u}) + \rho(\mathbf{u}\cdot\nabla)\mathbf{u} = -\nabla p + \eta\nabla^2\mathbf{u} + \zeta\nabla(\nabla\cdot\mathbf{u}). \tag{11}$$

The viscous term and the convective term are present and have the usual structure. The pressure p, shear viscosity η and the bulk viscosity ζ are found to be

$$p = \rho/2; \quad \eta \equiv \rho\nu = -\tfrac{1}{8}\rho c_\nabla^{(2)}; \quad \zeta = 0. \tag{12}$$

Actually, the extra term in (6b), which is proportional to $\nabla|u|^2$ can be combined with the $\nabla\rho$ term to yield an effective pressure which includes fluid kinetic energy contributions, i.e.,

$$p' = p - \tfrac{1}{8}\rho c^{(2)}|u|^2. \tag{13}$$

Further, the coefficient $c^{(2)}/4$ in the convective term can be absorbed in a rescaled velocity as

$$\mathbf{u}' = c^{(2)}\mathbf{u}/4, \tag{14}$$

so that (6b) reduces to the proper incompressible limit of the NS equation.

Then, the Reynolds number of the flow is given by

$$\mathrm{Re} = \mathbf{u}L\rho c^{(2)}/(4\eta). \tag{15}$$

The speed of sound is found to be isotropic and is

$$c = 1/\sqrt{2}. \tag{16}$$

The coefficient $c_V^{(2)}$, which determines the viscosity coefficients, can be calculated using an approximation method based on the Boltzmann transport equation. (Of course, it can also be found readily by explicit simulation.) In this, as in the standard case, the collision term Ω_a is assumed to be expressible totally in terms of the 1-particle distribution function f_a alone. The results, which are expected to be accurate at low particle densities are

$$\eta = 1/[2(1-f)^3] - 3f/4; \quad \zeta = 0, \tag{17}$$

where $f = \rho/6$. The negative contribution to η is a correction term (Henon 1987) due to the discrete nature of the lattice gas. The values of the viscosities will depend on the details of the collisions (this can be seen in the results, given below, for models II and III, which differ from each other only in the collision rules).

The results for models II and III which are both 7-particles/site models as described earlier in this section, are

$$p = 3\rho/7, \quad c = (3/7)^{1/2}, \tag{18a}$$

and

$$c^{(2)} = [7(2\rho - 7)]/[3(\rho - 7)]. \tag{18b}$$

These are the same for both the models. The results for η and ζ however are different in the two, as expected. They are given by

$$\left.\begin{aligned} \eta &= 1/[4(1-f)^3(1-4f/7)] - 7f/8 \\ \zeta &= 1/[14(1-f)^4] - f/4 \end{aligned}\right\} \text{for model II,} \tag{19}$$

and

$$\left.\begin{aligned} \eta &= 1/[4(1-f)(1-8f+8f^2/7)] - 7f/8 \\ \zeta &= 1/[14(1-f)(1-2f+2f^2)] - f/4 \end{aligned}\right\} \text{for model III.} \tag{20}$$

5. Computer simulations on the FHP lattice gas automaton

In this section, we present the results of numerical simulations (Hayot & Raj Lakshmi 1989; for other references, see d'Humieres & Lallemand 1987) of the FHP model and some of its variants. Simulations have been performed to study relaxation towards thermodynamical equilibrium, measure transport coefficients and the speed of sound, and also to simulate various two-dimensional flows. Qualitatively, these yield the correct fluid dynamical behaviour at large scales, and also reproduce known moderate-Reynolds-number features. Some quantitative results of simulations for these models have also been obtained.

5.1 *Simulations obtained from other studies*

To the best of our knowledge, these computer experiments have been performed mainly using the FPS-164 computer (d'Humieres & Lallemand 1986; d'Humieres *et al* 1985), the Cellular Automaton Machine (CAM-6, -7) (Toffoli 1984), and the Connection Machine (Hillis 1984). We will not give the details of these machines here, but refer the reader to the original papers, references to which are given above. Before proceeding on to the results of actual simulations, we will first outline the general procedure used for computer simulations on the FPS-164 machine.

Simulations of the CA models on this machine were done using lattices of $\approx 10^6$ nodes/site with typical speeds of 10^6 updates per second. The evolution of the FHP lattice gas is computed using a two-step parallel iteration. During the first step, the post-collision state is computed using either (i) a look-up table (in the FHP case, the states are coded with 8 bits, 7 for the particles and 1 to choose between the two different possible head-on collisions; thus, each of the 64-bit words of the FPS accommodates 8 nodes), or (ii) a combination of Boolean operators giving the collision rules (in this case, 64 nodes are packed into a word and 7 words are used to code the different particles; the choice between the head-on collisions is made randomly at each time-step). During the second step, the bits coding the different particles are moved from one node to the next one. The boundary conditions used at lattice edges and on obstacles have already been discussed in the last section. Initial flows are generated by a Monte Carlo procedure with the average population f_a related to the local velocity **u** by the equilibrium (local) distribution function given in (8). Macroscopic quantities are obtained by averaging the f_a according to (5) over regions with shapes and sizes adapted to the particular flow being studied.

The results of various simulations are:

(i) Relaxation to thermodynamic equilibrium has been demonstrated (Salem & Wolfram 1986) for the FHP model I. Figure 10 shows the approach towards equilibrium – the system randomizes and coarse-grained entropy increases with time. The initial state (configuration) used had a 100% occupancy in the middle of the lattice, and a much lower occupancy elsewhere. Starting from such non-equilibrium distributions, the relaxation to equilibrium proceeds on a time-scale of a few interaction times.

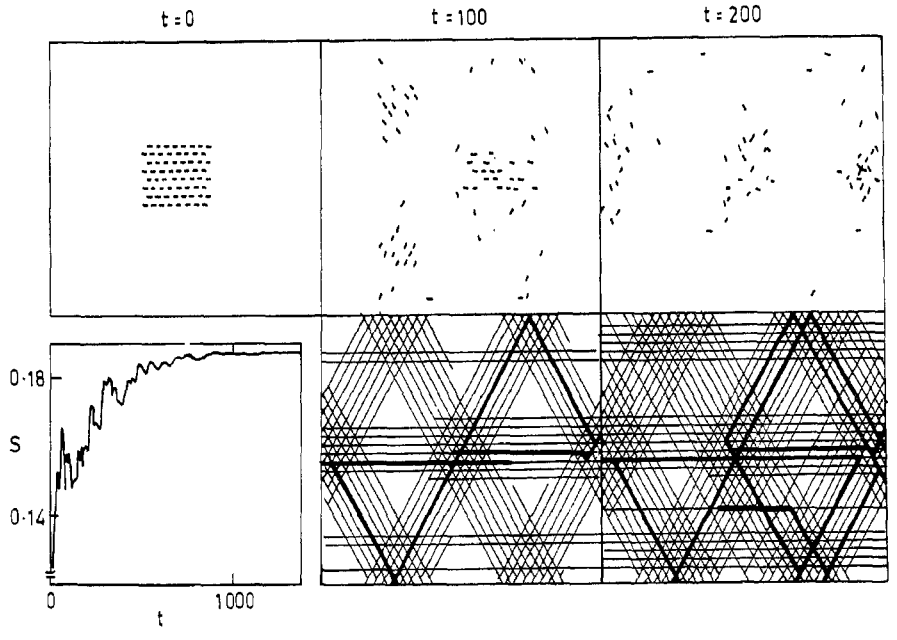

Figure 10. Relaxation to "thermodynamic equilibrium" in the FHP model I. Particles are initially in a simple array in the centre of a 32×32 site square box. The upper sequence shows the randomization of this pattern with time. The lower sequence shows the sites visited in the discrete phase space. The graph illustrates the resulting increase of coarse-grained entropy $\sum_i p_i \log_2 p_i$ calculated from particle densities in 32×32 regions of a 256×256 box.

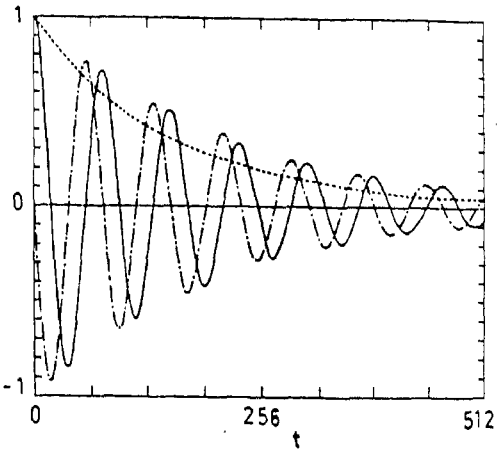

Figure 11. Time evolution of $u_\perp$(···), $u_\parallel$ (——) and ρ(–·–·–) normalized by the initial values of the velocity components.

(ii) The linear hydrodynamic region has been simulated to obtain the velocity of sound c, and the transport coefficients η and ζ (d'Humieres & Lallemand 1986; d'Humieres *et al* 1985a). These are measured by studying the relaxation of a periodic perturbation $(\mathbf{u}_\parallel + \mathbf{u}_\perp)\cos(\mathbf{k}\cdot\mathbf{r})$ of the velocity $\mathbf{u}$ field. From linear hydrodynamics, one knows that the relaxation of $\mathbf{u}$ depends on η and ζ, while the relaxation of the density $\delta\rho$ depends on η, ζ and c. Therefore, starting with an initial configuration corresponding to the above perturbation of the velocity field, the quantities c, η, ζ can be obtained by a least squares fit of the numerically simulated relaxation curves (see figure 11) to the known (expected) relaxation equations.

The measured sound velocities are isotropic (though the underlying world is anisotropic) and agree with the theoretical values of $1/(2)^{1/2}$ for model I and $(3/7)^{1/2}$ for models II and III.

The measured values of the viscosities are summarized in figure 12, along with the theoretical curves computed using (17), (18) and (19). The measured viscosities are seen to agree with theoretical predictions for models II and III. Without rest particles, i.e., in model I, the experimental (computer) values of η are too high. Thus, the presence of rest particles seems to improve the qualitative behaviour of the lattice gas while decreasing the viscosity significantly. Correspondingly, one would expect the Reynolds number for model III to be the highest. Figure 13 shows the achievable Reynolds number for the different FHP models for $uL = 1$; the maximum value is indeed obtained with model III and is six times larger than the maximum value for the original FHP model (model I).

These results show that the Reynolds numbers depend not only on the number of nodes (or sites) in the lattice, as observed in Frisch *et al* (1986) and d'Humieres *et al* (1986), but also on the details of the lattice gas CA models. The maximum achievable Reynolds numbers are of $O(10^3)$ at present.

(iii) Several simple non-linear flows have been simulated with the FHP model and its variants. The output is obtained generally by averaging over square regions containing either 16^2 or 32^2 sites. The Reynolds number is varied by changing the hydrodynamic speed and the size of obstacles. These simulations were only meant to verify the global qualitative features. Here we give the results for some of the simulated flows:

(a) A quasi-steady recirculating flow past a "specular" flat plate (i.e., at which specular boundary conditions were used) placed normal to the flow was simulated (d'Humieres *et al* 1985a). The lattice, which had 1024 × 1024 sites was wrapped around periodically.

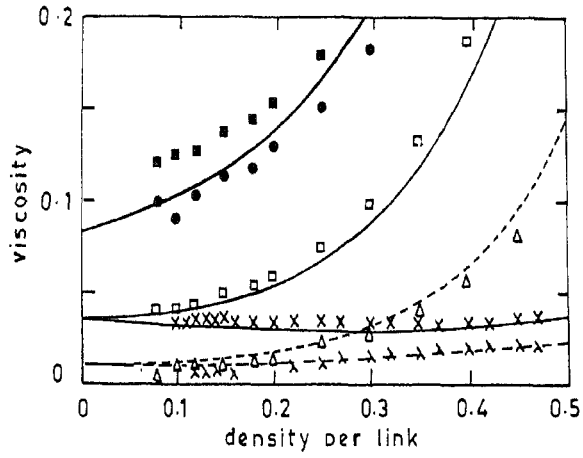

Figure 12. Theoretical shear (——) and bulk (– – –) reduced viscosities (=viscosity $\times f/\rho$) as a function of the reduced density ($=f$; $=\rho/6$ for model I, and $=\rho/7$ for models II, III). Also shown are results of numerical simulations for different models: original FHP model I (■, ●), model II with rest particles and limited collisions (□, △), and model III with rest particles and all possible collisions (×, ×).

Figure 14 shows the vortices in such a flow. The mean flow was 0·35 (in units of molecular velocity) and the density $\rho = 1{\cdot}02$. This was done using model I, i.e., the original FHP model with no rest particles.

(b) Two vortices resulting from a Kelvin–Helmholtz instability are shown in figure 15. This was simulated by first establishing two quasi-uniform thermalized regions of opposite mean flow, separated by a period two (i.e., two time steps) sinusoidal "specular" barrier. After 200 time steps, the barrier was removed and the flows allowed to mix freely.

(c) A von Karman vortex street (d'Humieres *et al* 1985; d'Humieres & Lallemand 1986) behind a "bounce-back" flat plate kept normal to the flow is shown in figure 16 (in figure 16b, the mean flow has been subtracted). This is only a "snapshot" (the flow is actually time-dependent) taken after 5000 time steps and the Reynolds number of the flow was ≈ 90. The vortex street at a later time (after 6500 time steps) is shown in figure 17. The mean flow was of velocity 0·51 (in units of molecular velocity) and was generated in a 1024×512 "wind-tunnel". As mentioned earlier, this overall flow is obtained by maintaining a difference in the numbers of left- and right-moving particles at the boundaries. Since local equilibrium is rapidly reached from almost any state, the results are insensitive to the precise arrangement used. Reflecting or

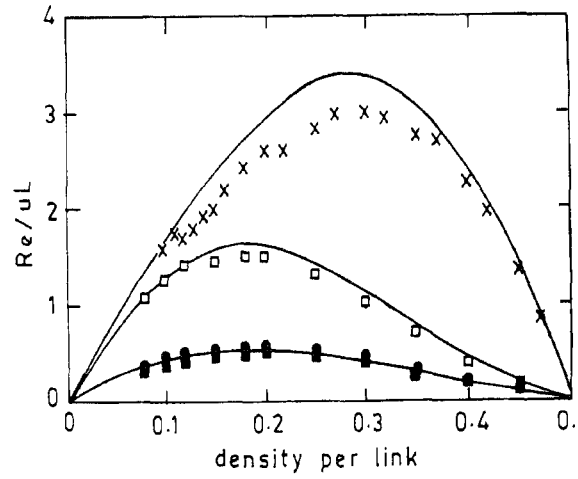

Figure 13. Achievable Reynolds number as a function of the reduced density (——: theory; symbols: measured values) for the different models, with the same symbols as in figure 12.

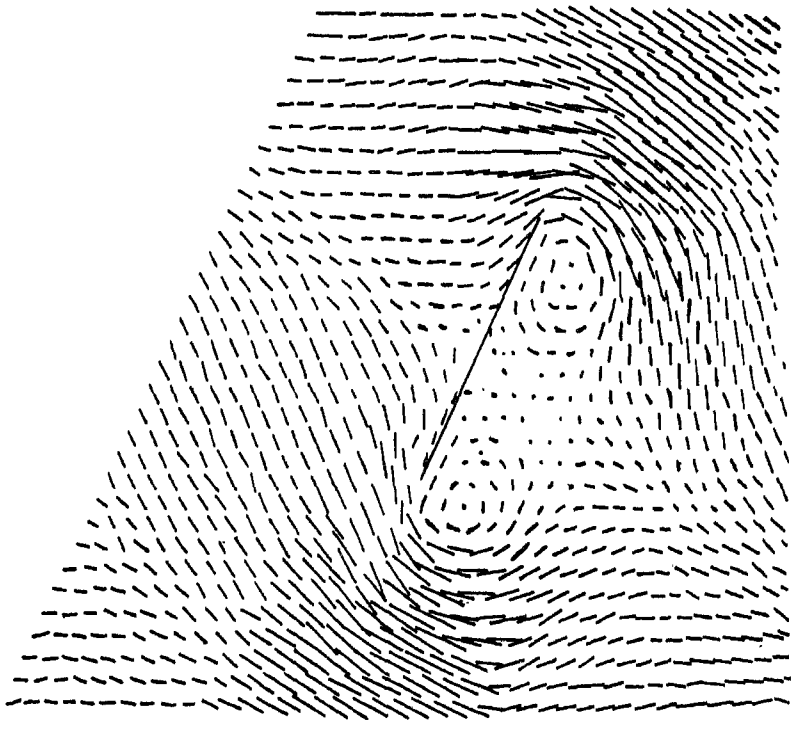

Figure 14. Recirculating flow behind a flat plate at 1000 time steps.

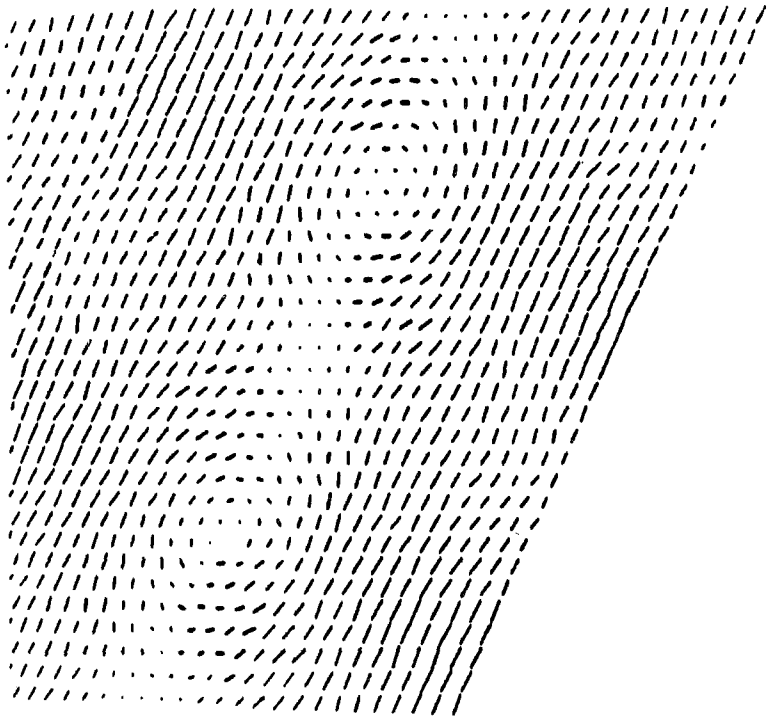

Figure 15. Vortices resulting from a Kelvin–Helmholtz instability at 780 time steps.

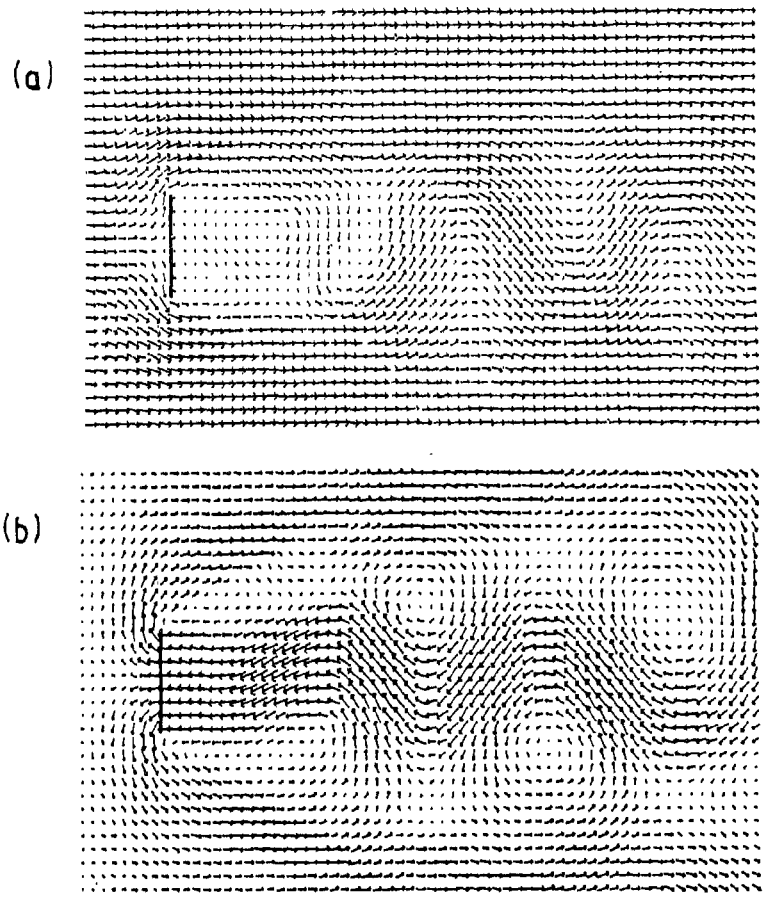

Figure 16. Von Karman vortex street behind a flat plate at 5000 time steps with "wind tunnel" boundary conditions at Re=80, shown in (**a**) as such, in (**b**) with mean flow subtracted.

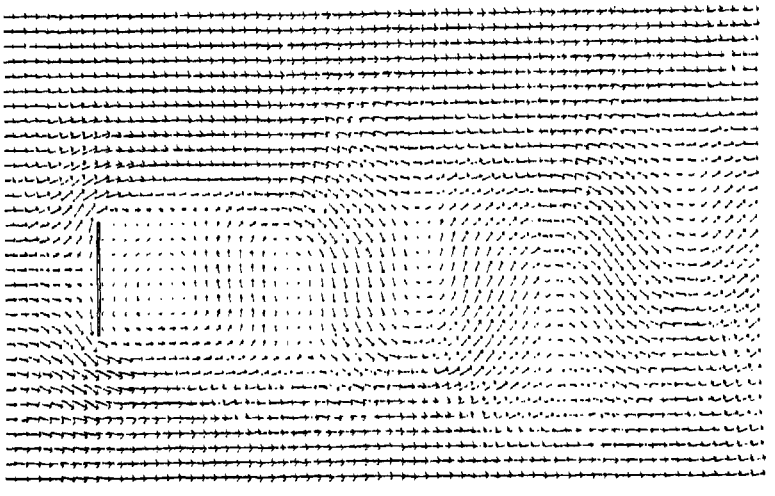

Figure 17. Flow under the same conditions as in figure 16a, but 1500 time steps later, i.e., at 6500 time steps.

cyclic boundary conditions are used on the top and bottom edges of the lattice. The lattice gas model used was model II which has rest particles. The density ρ was chosen to be 1·4 so as to maximize the Reynolds number, and the length L of the plate was 120.

Figure 18 shows the flow behind the plate as a function of time (here the mean flow has not been subtracted), and figure 19 shows it as a function of the Reynolds number (Nemnich & Wolfram 1986; Salem & Wolfram 1986). At low Re, the flow is macroscopically stable, while at higher Re, vortex streets are produced.

(d) The flow behind a moving cylinder in the CA fluid is shown in figure 20 (Nemnich & Wolfram 1986). This also seems to be correct, qualitatively at least. Subsonic and locally supersonic flows around a stationary cylinder in the CA fluid model have also been studied. Results are shown in figure 21 (Nemnich & Wolfram 1986).

5.2 *Our simulations on a 2-D cylinder wake*

In this subsection, we present the results of our work (Hayot and Raj Lakshmi 1989) on the wake of a cylinder in two-dimensional lattice-gas hydrodynamics. The model used was the FHP model I and the wake was investigated at low and moderate Reynolds numbers ($30 \leqslant Re \leqslant 200$).

At $Re = 30$ and 60, we studied the time development of the wake, and compared it to available experimental results. The wake initially increased linearly in time and later reached a steady length. Our results on the linear part, which we found to depend on the Reynolds number, were in reasonable agreement with experiments. At $Re = 30$, the final steady length was attained earlier than that shown by the experimental data and its value was 15% lower. At $Re = 60$, the maximum wake length was reached at a later time and was higher than the one at $Re = 30$, again in agreement with experimental results.

We also measured the drag on the cylinder at $Re = 30$ and 60. The longitudinal force on the cylinder was obtained simply by adding the momenta (in the longitudinal direction) t. ansferred to the cylinder when particles bounced off its surface, in a time step. This calculation is a trivial matter in lattice-gas hydrodynamics. Our results were lower than other numerical ones by about 20%, but the qualitative trend of decreasing drag with increasing Reynolds number was present.

As we increased the Re, we found that the above-mentioned low-Re behaviour of the wake continued only upto $Re = 90$, at which Re, there was an instability leading to vortex shedding by the cylinder. Therefore, we were able to measure a Strouhal number at $Re = 108$, where experimental results are available.

We did this by determining the time dependence of the transverse velocity (i.e. perpendicular to the flow) at a point on the axis behind the cylinder. As expected, results were independent of where this point was located on the axis. The velocity was found to be periodic, and we obtained a Strouhal number (inversely proportional to the time period) of 0·3. This is roughly 50% higher than the experimental value.

We also measured the Strouhal number by another method, namely from the lift (transverse force) exerted by the flow on the cylinder. This we did at $Re = 180$. The lift was simply computed by adding the transverse moment per unit time step transferred to the cylinder by particles bouncing off its surface. We found that the lift was periodic in time, as per our expectations. The Strouhal number calculated from this time period was consistent with the value obtained from the transverse velocity measurements, and therefore too large compared to the experimental value. We found, however, that the Strouhal number depended on the ratio of the cylinder

Figure 18. Time evolution of flow behind a flat plate in the FHP model I on a 2048 × 2048 lattice. Hydrodynamic velocities are obtained by averaging over 64 × 64 site regions. The microscopic forms of 20 × 30 parts of two such regions are shown. The average density is 0·3 particles per link and the mean flow (overall velocity) is 0·1.

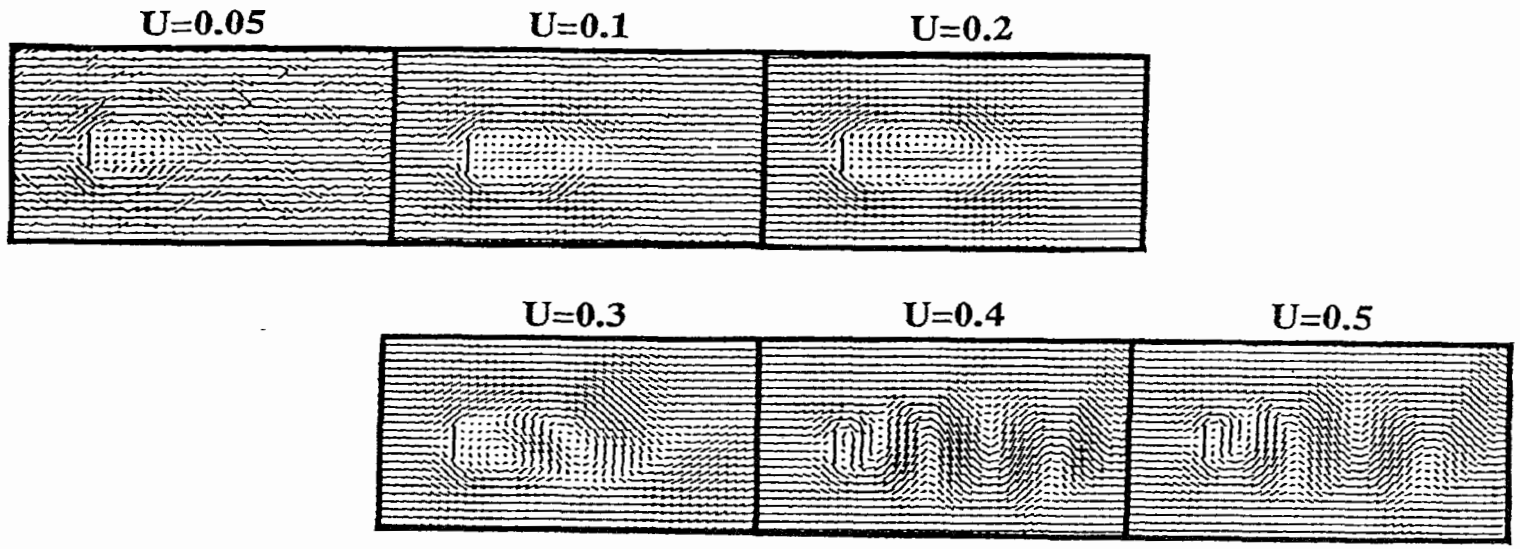

Figure 19. Flows behind a flat plate obtained after 10 time steps in the CA of figure 18, for various overall velocities, i.e., as a function of the Reynolds number.

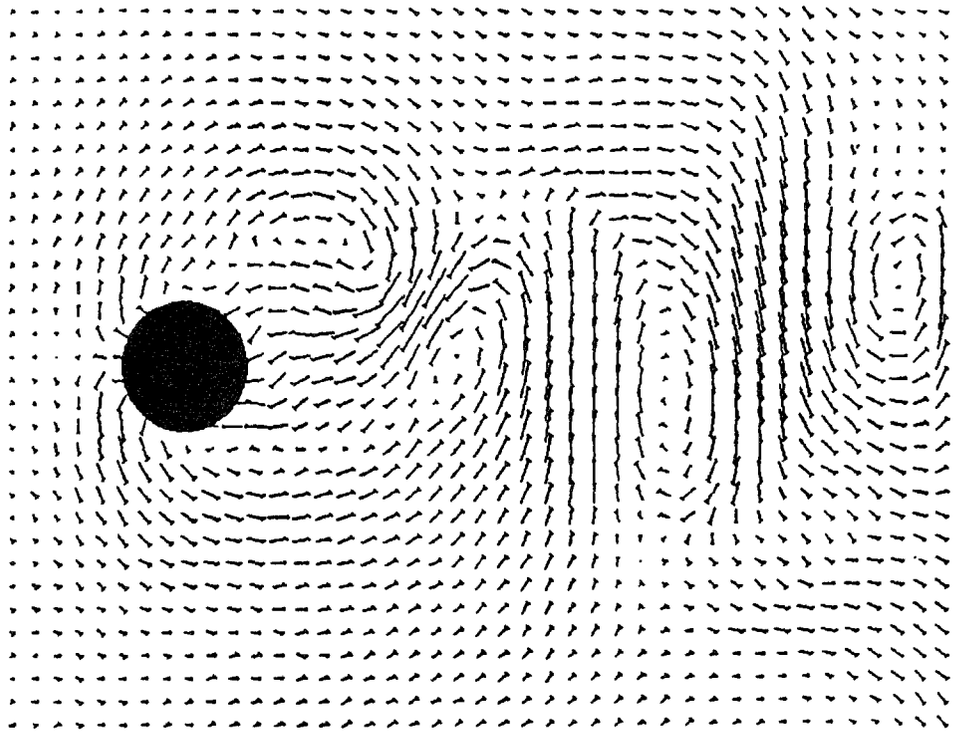

Figure 20. Flow behind a moving cylinder in a cellular automaton fluid.

diameter to the system width, with periodic conditions across the width. It decreased towards the experimental value as this ratio was decreased.

All these simulations were performed on a VAX 8600, and the details of this work are given in Hayot & Raj Lakshmi (1989).

6. Details of derivation of macrodynamical equations for the FHP model

The results for this model have already been given in §4. Here we discuss all the details of the derivation of the equations describing the macroscopic behaviour of this model; these are taken mostly from Wolfram (1986). The derivation uses standard methods from kinetic theory to show that the macroscopic behaviour of the FHP model corresponds to the standard Navier–Stokes equations for fluid flow. The form of the macroscopic equations depends only on a few general features of the CA model, such as the symmetry of the lattice. Details at the macroscopic level, such as changes in the collision rules do not alter the basic form of these equations; they only affect parameters such as viscosity.

6.1 *Kinetic equations*

In studying macroscopic phenomena, it is convenient to consider reduced distribution functions (rather than the full phase-space distribution function), for example, the one-particle distribution function $f_a(\mathbf{x}, t)$. This gives the probability of finding particles

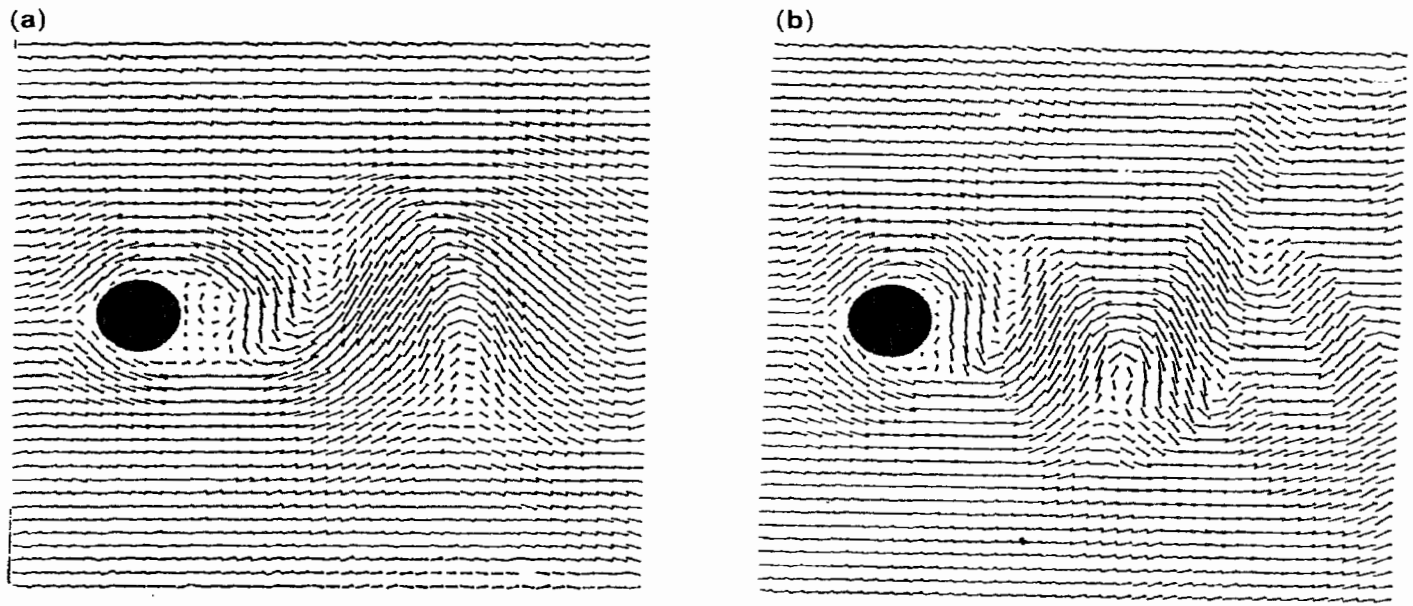

Figure 21. Subsonic (a) and locally supersonic (b) flows around a stationary cylinder in a cellular automaton fluid.

with velocity $\hat{e}_a$ at position $\mathbf{x}$ and time t. Changes in f_a with time can arise from two processes: translations and collisions. This can be described by the master equation:

$$\partial_t f_a(\mathbf{x}, t) + \hat{e}_a \cdot \nabla f_a(\mathbf{x}, t) = \Omega_a. \tag{21}$$

In the absence of collisions ($\Omega_a = 0$), this has the form of a collisionless Boltzmann transport equation for f_a. The effect on f_a of collisions can be complicated; it is summarized in the term Ω_a. The details of this term are not important for the present; we will only assume it to be local. Actually, higher order (in ∂_t and ∇) corrections to (21) are present due to the discreteness of space and time, but we will not go into that.

6.2 *Conservation laws*

The macroscopic average quantities such as the particle density ρ and the momentum density $\rho\mathbf{u}$ (where $\mathbf{u}$ is the average fluid velocity) are determined in terms of the function f_a as

$$\rho = \sum_a f_a, \tag{22}$$

$$\rho\mathbf{u} = \sum_a \hat{e}_a f_a. \tag{23}$$

We will now obtain evolution equations for these average quantities, assuming slow variations with position and time. Since collisions conserve particle number and momentum, it follows that

$$\sum_a \Omega_a = 0, \tag{24a}$$

$$\sum_a \hat{e}_a \Omega_a = 0. \tag{24b}$$

Using the kinetic equation (21), (24a) implies

$$\partial_t \sum_a f_a(\mathbf{x}, t) + \sum_a \hat{e}_a \cdot \nabla f_a(\mathbf{x}, t) = 0. \tag{25}$$

This can be written exactly in terms of macroscopic quantities as

$$\partial_t \rho + \nabla \cdot (\rho\mathbf{u}) = 0. \tag{26}$$

This is the usual continuity equation, which expresses the conservation of fluid.

Momentum conservation, i.e. (24b), together with (21) yields

$$\partial_t \sum_a \hat{e}_a f_a + \sum_a \hat{e}_a (\hat{e}_a \cdot \nabla f_a) = 0 \tag{27}$$

which can be expressed in terms of the momentum flux density tensor π_{ij} as

$$\partial_t(\rho\mathbf{u}_i) + \partial_j \pi_{ij} = 0 \tag{28}$$

with

$$\pi_{ij} \equiv \sum_a (\hat{e}_a)_i (\hat{e}_a)_j f_a. \tag{29}$$

Here, unlike before, no simple macroscopic result can be obtained directly from (22) and (23). Corrections to the transport equation (21) arising from the discreteness of

space-time will also be present in (26) and (28) since these have been derived from (21). However, it is found that lattice and time discretization effects do not affect the continuity equation (26), at least to second order; but they do give a correction to the momentum equation (28). We will not give details of these corrections here. Now, π_{ij} has to be expressed in terms of the macroscopic quantities.

6.3 *Chapman-(Enskog) expansion*

For this, we note that if there is local equilibrium, then the distribution functions $f_a(\mathbf{x}, t)$ should depend only on the macroscopic quantities $\mathbf{u}(\mathbf{x}, t)$ and $\rho(\mathbf{x}, t)$ and their derivatives. Further, in hydrodynamic processes, $\mathbf{u}$ and ρ vary only slowly with position and time. In addition, in the subsonic limit (i.e. low Mach nos.), we have $|\mathbf{u}| \ll 1$.

Then we can make a Chapman expansion for f_a as (to the order required)

$$f_a = f\{1 + c^{(1)}\hat{e}_a\cdot\mathbf{u} + c^{(2)}[(\hat{e}_a\cdot\mathbf{u})^2 - \tfrac{1}{2}|\mathbf{u}|^2] + c_\nabla^{(2)}[(\hat{e}_a\cdot\nabla)(\hat{e}_a\cdot\mathbf{u}) - \tfrac{1}{2}\nabla\cdot\mathbf{u}] + \cdots\}, \tag{30}$$

where $c^{(i)}$ are undetermined coefficients and are functions of ρ. (Contrast this with the usual Chapman–Enskog expansion for $f(\mathbf{v}, \mathbf{r}, t)$, where one expands only in the gradients of the velocity and not in the velocity itself.) The structures of the terms can be deduced merely from the need to form scalars out of the vectors $\hat{e}_a$, $\mathbf{u}$ and ∇. The coefficients of the $|u|^2$ and $(\nabla\cdot\mathbf{u})$ terms have been chosen so that f_a satisfies (22) and (23) independent of the values of $c^{(2)}$ and $c_\nabla^{(2)}$. Further, the same two equations yield respectively

$$f = \rho/6 \quad \text{and} \quad c^{(1)} = 2. \tag{31}$$

In the above, use has been made of the relation

$$\sum_a (\hat{e}_a)_i(\hat{e}_a)_j = (M/d)\delta_{ij} \tag{32}$$

where $M = 6$ (number of unit vectors $\hat{e}_a$) and $d = 2$ (space dimension) in our case; i, j are space indices. The specific values of $c^{(2)}$ and $c_\nabla^{(2)}$ are not needed to derive the structure of the macroscopic equations. We will therefore defer that calculation for now.

For a uniform equilibrium system (i.e. $\mathbf{u} = 0$),

$$f_a = f = \rho/6, \tag{33}$$

and the pressure tensor, which is nothing but the momentum flux density tensor in this case, is given by (as in the standard theory of gases)

$$P_{ij} = \sum_a (\hat{e}_a)_i(\hat{e}_a)_j f = \frac{\rho}{2}\delta_{ij}. \tag{34}$$

(Remember that for the standard case, the correspondences are $\hat{e}_a \leftrightarrow \mathbf{v}$, $\sum_a \leftrightarrow \int d\mathbf{v}$ etc.). Note that P_{ij} is spatially isotropic; actually, this can be deduced from general symmetry considerations alone. From (34) we get the equation of state for the CA fluid to be:

$$p = \rho/2. \tag{35}$$

When $\mathbf{u} \neq 0$, the approximation for f_a given in (30) can be used to evaluate π_{ij}. Substituting for f_a in the definition (29) for π_{ii}, we get

$$\pi_{ij} = f(E^{(2)}_{ij} + c^{(1)}E^{(3)}_{ijk}u_k + c^{(2)}[E^{(4)}_{ijkl}u_k u_l + \sigma E^{(2)}_{ij}u_k u_k] + c^{(2)}_{\nabla}[E^{(4)}_{ijkl}\partial_k u_l + \sigma E^{(2)}_{ij}\partial_k u_k]), \tag{36}$$

where

$$E^{(n)}_{i_1 i_2, \ldots, i_n} = \sum_a (\hat{e}_a)_{i_1}(\hat{e}_a)_{i_2}, \ldots, (\hat{e}_a)_{i_n}, \tag{37}$$

and σ is taken to be equal to $-E^{(4)}_{ijkk}/E^{(2)}_{ij}$ to satisfy relations (22) and (23). Using the relation (32) for $E^{(2)}$ and the relations

$$\sum_a (\hat{e}_a)_i(\hat{e}_a)_j(\hat{e}_a)_k = 0, \tag{38}$$

$$\sum_a (\hat{e}_a)_i(\hat{e}_a)_j(\hat{e}_a)_k(\hat{e}_a)_l = [M/d(d+2)]\,(\delta_{ij}\delta_{kl} + \delta_{ik}\delta_{jl} + \delta_{il}\delta_{jk}), \tag{39}$$

in (36), we get for π_{ij} the result

$$\pi_{ij} = (\rho/2)\delta_{ij} + (\rho/4)c^{(2)}[u_i u_j - \tfrac{1}{2}|u|^2\delta_{ij}] + (\rho/4)c^{(2)}_{\nabla}[\partial_i u_j - \tfrac{1}{2}\nabla\cdot\mathbf{u}]. \tag{40}$$

Substituting this into (28), we get the final macroscopic equation for the momentum density

$$\partial_t(\rho\mathbf{u}) + \tfrac{1}{4}\rho c^{(2)}\{(\mathbf{u}\cdot\nabla)\mathbf{u} + [\mathbf{u}(\nabla\cdot\mathbf{u}) - \tfrac{1}{2}\nabla|\mathbf{u}|^2]\} = -\tfrac{1}{2}\nabla\rho - \tfrac{1}{8}\rho c^{(2)}_{\nabla}\nabla^2\mathbf{u} - \tfrac{1}{4}\Theta, \tag{41}$$

where

$$\Theta = \mathbf{u}(\mathbf{u}\cdot\nabla)(\rho c^{(2)}) - \tfrac{1}{2}|u|^2\nabla(\rho c^{(2)}) + (\mathbf{u}\cdot\nabla)(\rho c^{(2)}_{\nabla}) - \tfrac{1}{2}(\nabla\cdot\mathbf{u})\nabla(\rho c^{(2)}_{\nabla}). \tag{42}$$

Corrections arising from the discreteness of the lattice add a term $-\rho\nabla^2\mathbf{u}/8$ to the RHS of (41).

6.4 *Navier–Stokes equation*

Equation (41) has to be compared with the standard Navier–Stokes equation for a continuum fluid, which in d dimensions (here $d=2$) can be written as

$$\partial_t(\rho\mathbf{u}) + \rho(\mathbf{u}\cdot\nabla)\mathbf{u} = -\nabla p + \eta\nabla^2\mathbf{u} + \{\zeta + [(d-2)/d]\eta\}\nabla(\nabla\cdot\mathbf{u}). \tag{43}$$

Examining the macroscopic equation (41) for the CA fluid, we find that convective and viscous terms are present and that the pressure term appears according to the equation of state (35).

However, there are some additional terms. Note that in writing (41), we have implicitly made the assumption of incompressibility, because gradients of ρ have not been retained except in the pressure term (which is the usual practice). Thus, consistently, we must neglect the terms proportional to $\mathbf{u}\cdot\nabla\rho$, which are collectively denoted by Θ in (42). Another reason for discounting these terms is that they depend on features of the microscopic distribution function f_a beyond those included in the Chapman–Enskog expansion, (30). Also, the term proportional to $\mathbf{u}(\nabla\cdot\mathbf{u})$ must be neglected for consistency with the condition of incompressibility.

The term which is proportional to $\nabla|\mathbf{u}|^2$ however remains. It can be combined

with the $\nabla\rho$ term to give an effective pressure

$$p' = (\rho/2) - (1/4)\rho c^{(2)}|u|^2. \tag{44}$$

This means that the pressure depends on the macroscopic velocity $\mathbf{u}$ which in turn implies that the pressure depends on the frame of reference; this is not a very desirable feature and has to be investigated further.

Comparing the viscous terms in (41) and (43), we find that for this cellular automaton fluid, the bulk viscosity is

$$\zeta = 0, \tag{45}$$

and the shear viscosity is given by

$$\eta \equiv \rho\nu = -(1/8)\rho c_\nabla^{(2)}. \tag{46}$$

where ν is the kinematic viscosity. An approximate method of evaluating $c_\nabla^{(2)}$ will be presented later in this section.

The convective term in (41) has the correct structure but it has a coefficient

$$(1/4)c^{(2)}(\rho) \equiv \mu \neq 1. \tag{47}$$

But Galilean invariance demands that this coefficient be unity. This can be easily achieved by rescaling velocity as

$$\mathbf{u}' = \mu\mathbf{u} = (1/4)c^{(2)}\mathbf{u}. \tag{48}$$

Then the equation for $\mathbf{u}'$ has a coefficient of unity for the $(\mathbf{u}'\cdot\nabla)\mathbf{u}'$ term.

The speed of sound in this CA fluid can be obtained as usual by considering small perturbations from a uniform state. These can be represented by a linearized approximation to (26) and (41), which yields the standard sound-wave equation. The speed of sound obtained from the equation of state (35) is

$$c = 1/\sqrt{2}. \tag{49}$$

6.5 *Higher order corrections*

The derivation of the macroscopic equation (41) neglects all terms in the Chapman–Enskog expansion beyond those given explicitly in (30). This approximation is expected to be adequate only at low Mach numbers, i.e. when $|\mathbf{u}| \ll c$. Higher order corrections may be particularly significant for transonic and supersonic flows involving shocks. In both cellular automaton fluids and in standard continuum fluids, the dynamics of shocks are expected to be closely analogous, because they are determined mainly by just the conservation laws. Now in the transonic flow regime $|\mathbf{u}| \simeq c$, one may continue to use continuum equations; however, corrections to the Navier–Stokes form of the macroscopic equations (41) may be significant. These corrections can actually be found by keeping terms of $O(|u|^3)$ and higher in the Chapman–Enskog expansion for f_a, but we will not go into any more details here.

6.6 *Evaluation of the coefficient $c^{(2)}$*

The coefficient $c^{(2)}(\rho)$ can be obtained by comparing the Chapman–Enskog expansion (30) with the local equilibrium one-particle distribution function f_a. The latter is

obtained by using Boltzmann's H-theorem. The H-function can be defined as

$$H = \sum_a \tilde{f}_a \ln(\mathbf{f}_a) \tag{50}$$

where

$$\tilde{f}_a = f_a/(1-f_a). \tag{51}$$

This definition is analogous to that used for Fermi–Dirac particles; the exclusion of more than one particle on each link is taken into account via the factors $(1-f_a)$. If we use the equilibrium condition $\partial_t H = 0$ together with the conservation of particle number and momentum in collisions (there should be no other spurious conserved quantities), we can write $\tilde{f}_a$ in the form

$$\tilde{f}_a = \exp[-\alpha - \gamma \mathbf{u}\cdot\hat{e}_a], \tag{52}$$

where α, γ are the Lagrange multipliers and are in general, functions of ρ and $|u|^2$. Thus the one-particle distribution functions f_a are

$$f_a = \{1 + \exp[\alpha(\rho, |\mathbf{u}|) + \gamma(\rho, |\mathbf{u}|\mathbf{u}\cdot\hat{e}_a]\}^{-1}. \tag{53}$$

This has the expected Fermi–Dirac form.

We can expand α and γ in powers of $|u|^2$ as

$$\alpha = \alpha_0 + \alpha_1 |u|^2 + \cdots; \quad \beta = \beta_0 + \beta_1 |u|^2 + \cdots. \tag{54}$$

Substituting these into (53) and comparing the results with the Chapman–Enskog expansion (30), we find immediately that

$$\exp(-\alpha_0) = f/(1-f), \tag{55a}$$

and

$$c^{(2)} = [d^2(1-2f)]/[2(1-f)] = 4(3-\rho)/(6-\rho) \tag{55b}$$

for the FHP model I ($f = \rho/6$) in two dimensions.

6.7 *Evaluation of the coefficient $c_\nu^{(2)}$ (and hence of the viscosity coefficients)*

Though these coefficients can readily be found by explicit simulation, as discussed in §5 there is no exact analytical procedure for calculating them. We therefore consider an approximate method based on the Boltzmann transport equation. The results are expected to be valid at low particle densities when the assumption of absence of correlations between particles is reasonable.

The collision term Ω_a in the kinetic equation (21) in general depends on two-particle distribution functions, which in turn depend on higher order distribution functions. Thus (21) for f_a leads to the usual BBGKY (Bogoliubov, Born, Green, Kirkwood & Yvon) hierarchy of kinetic equations; one must truncate these equations (by a suitable closure approximation) to obtain explicit results for f_a.

As in the standard case, if we assume that there are no statistical correlations between particles participating in any collision, then we can express the multiparticle distribution functions in Ω_a as products of one-particle distribution functions f_a. The resulting equation will be of the standard Boltzmann transport form. Here we will describe the formulation of the Boltzmann transport equation for the original FHP model (but with all possible collision rules, shown in figure 8), and then make the linear approximation to it to calculate $c_\nu^{(2)}(\rho)$.

Figure 8 shows the possible classes of particle collisions; the rules for different collisions within each class are related by lattice symmetries. But, even within a class, there can be several choices of overall rules; for example, the 2-particle collisions can lead to two different outputs, $2L$ and $2R$. To allow for this, we apply a set of rules denoted by k at some fraction γ_k of the sites in the CA lattice. Thus, the γ_k serve merely to change the overall probabilities for different types of collisions.

Now the collision term Ω_a which is actually a sum of terms representing possible collisions involving particles of type a, has to be written down in the Boltzmann transport equation approximation. Each term in Ω_a gives the change in the number of type a particles due to a particular type of collision, multiplied by the probability of occurrence of such a configuration. Under the 'molecular chaos' approximation, this probability is just the product of the densities f_a for particles that should be present (for the collision to take place) and the factors $(1-f_a)$ for particles that must be absent. Thus for the above model, we have

$$\begin{aligned}\Omega_a = {} & [\gamma_{2L}\Lambda_a(1,4)+(\gamma_2-\gamma_{2L})\Lambda_a(2,5)]-\gamma_2\Lambda_a(0,3)+\\ & +\gamma_{3S}[\Lambda_a(1,3,5)-\Lambda_a(0,2,4)]+\\ & +\gamma_{3A}[\Lambda_a(2,4,5)+\Lambda_a(1,2,5)-\Lambda_a(0,3,5)-\Lambda_a(0,2,3)+\\ & \qquad +\Lambda_a(1,4,5)+\Lambda_a(1,2,4)-\Lambda_a(0,3,4)-\Lambda_a(0,1,3)]+\\ & +[\gamma_4\Lambda_a(1,2,4,5)-\gamma_{4L}\Lambda_a(0,2,3,5)-(\gamma_4-\gamma_{4L})\Lambda_a(0,1,3,4)],\end{aligned} \tag{56}$$

where

$$\gamma_2=\gamma_{2R}+\gamma_{2L},\quad \gamma_4=\gamma_{4R}+\gamma_{4L};$$

$$\Lambda_a(i_1,i_2,\ldots,i_k)=\frac{f_{a+i_1}}{(1-f_{a+i_1})}\cdot\frac{f_{a+i_2}}{(1-f_{a+i_2})}\cdots\cdots\frac{f_{a+i_k}}{(1-f_{a+i_k})}\prod_{j=1}^{M}(1-f_{a+j}); \tag{57}$$

the indices on the f's are evaluated modulo M (here $M=6$).

As in the Chapman–Enskog expansion, we make the assumption that the f_a differ only slightly from their equilibrium values (justified when macroscopic behaviour is being studied) and write

$$f_a=f(1+\phi_a),\quad |\phi_a|\ll 1. \tag{58}$$

Then the Ω_a term can also be approximated by a power-series expansion in ϕ_a, as

$$\Omega_a=\sum_b \omega^{(1)}_{ab}\phi_b+\sum_{b,c}\omega^{(2)}_{abc}\phi_b\phi_c+\cdots. \tag{59}$$

The matrix $\omega^{(1)}_{ab}$ is the usual linearized collision operator. This is all that we need to evaluate the coefficient $c^{(2)}_{\nabla}$ ($\omega^{(2)}_{abc}$ is not needed).

Equation (56) for Ω_a can be expanded in powers of ϕ using the expansion (58) for f_a. The matrix coefficient of the linear term will be $\omega^{(1)}_{ab}$. Since the expressions for the matrix elements are lengthy, we do not display them here. Note that $\omega^{(n)}_{(a+1)bc\ldots}$ is given simply by a cyclic shift of $\omega^{(n)}_{abc}$ because all particle types a are equivalent upto lattice symmetry transformations. The complete form of $\omega^{(n)}$ can be determined from just the first row $\omega^{(n)}_{1bc\ldots}$. In fact, the $\omega^{(n)}$ are the so-called circulant tensors.

We now use the microscopic equilibrium condition

$$\partial_t f_a=0, \tag{60}$$

in the Boltzmann transport equation,

$$\partial_t f_a + \hat{e}_a \cdot \nabla f_a = \Omega_a, \tag{61}$$

with Ω_a given by (59) and (56). Substituting the expansion (58) for f_a and keeping only first-order spatial derivatives of the ϕ_b, we get

$$\sum_b \omega_{ab}^{(1)} \phi_b = f \hat{e}_a \cdot \nabla \phi_a. \tag{62}$$

Using the Chapman–Enskog expansion (30) for the form of ϕ_b, in the above equation, we get

$$\sum_b c_\nabla^{(2)} \omega_{ab}^{(1)} (\hat{e}_b \cdot \nabla)(\hat{e}_b \cdot \mathbf{u}) = c^{(1)} f (\hat{e}_a \cdot \nabla)(\hat{e}_a \cdot \mathbf{u}). \tag{63}$$

This gives the result

$$c_\nabla^{(2)} = -2\{12f(1-f)[\gamma_2(1-f)^2 + 4\gamma_{3A} f(1-f) + \gamma_4 f^2]\}^{-1}; \tag{64}$$

in deriving the form (63) we have used the incompressibility condition $\nabla \cdot \mathbf{u} = 0$.

From this, using (46), we get the kinematic viscosity of the CA fluid in the Boltzmann transport equation approximation to be

$$\nu = \{12f(1-f)[\gamma_2(1-f)^2 + 4\gamma_{3A} f(1-f) + \gamma_4 f^2]\}^{-1}. \tag{65}$$

Some particular choices for the γ_k and the resulting values of ν are

$$\nu = [12f(1-f)^3]^{-1}, \quad (\gamma_2 = 1,\ \gamma_{3A} = \gamma_4 = 0 \Rightarrow \text{model I}), \tag{66a}$$

$$\nu = [12f(1-f)(1+2f-2f^2)]^{-1}, \quad (\gamma_2 = \gamma_{3A} = \gamma_4 = 1). \tag{66b}$$

For $\rho = 1$ (i.e. $f = 1/6$), we get $\nu \approx 0{\cdot}86$ and $\approx 0{\cdot}47$ for the values of γ given in (66a) and (66b) respectively. This clearly shows that, as more collisions are included, the viscosity decreases.

6.8 *Symmetry considerations*

Here we will discuss the symmetry properties of the tensors $E^{(n)}$ which are defined as before, as

$$E^{(n)}_{i_1 i_2 \ldots i_n} = \sum_a (\hat{e}_a)_{i_1} (\hat{e}_a)_{i_2} \cdots (\hat{e}_a)_{i_n}.$$

These tensors are determined in any cellular automaton fluid model simply from the choice of the basic particle directions $\hat{e}_a$. The momentum flux density tensor π_{ij} is given in terms of these by (36). It has the tensors $E^{(2)}$ and $E^{(4)}$. The basic condition for obtaining standard hydrodynamic behaviour is that the tensors $E^{(n)}$ for $n \leqslant 4$ which appear in (36) should be isotropic. This means that they should be invariant under the full continuous rotation group; they are by definition invariant under the discrete symmetry group of the underlying CA array.

Tensors which are isotropic can have only one independent component. In particular, the isotropic tensors $E^{(n)}$ obtained with sets of M vectors $\hat{e}_a$ in d space

dimensions must take the form

$$E^{(2n+1)} = 0,$$
$$E^{(2n)} = \{M/[d(d+2)\cdots(d+2n-2)]\}\Delta^{(2n)}, \tag{67}$$

where

$$\Delta^{(2)}_{ij} = \delta_{ij},$$
$$\Delta^{(4)}_{ijkl} = \delta_{ij}\delta_{kl} + \delta_{ik}\delta_{jl} + \delta_{il}\delta_{jk},$$

and in general, $\Delta^{(2n)}$ are given by the recursion relation

$$\Delta^{(2n)}_{i_1 i_2 \ldots i_{2n}} = \sum_{j=2}^{2n} \delta_{i_1 i_j} \Delta^{(2n-2)}_{i_2 \ldots i_{j-1} i_{j+1} \cdots i_{2n}}.$$

In *two space dimensions* (*2-D*), consider the set of unit vectors $\hat{e}_a$ corresponding to the vertices of a regular M-sided polygon:

$$\hat{e}_a = [\cos(2\pi a/M), \sin(2\pi a/M)].$$

We give below the conditions on M necessary to obtain an isotropic $E^{(n)}$:

$$\begin{aligned} &\text{for } E^{(2)}, \quad M > 2; \\ &\text{for } E^{(4)}, \quad M > 2,\ M \neq 4; \\ &\text{for } E^{(6)}, \quad M > 4,\ M \neq 6. \end{aligned} \tag{68}$$

For sufficiently large M, any tensor $E^{(n)}$ will be isotropic.

For a square lattice, $M = 4$. This gives an anisotropic $E^{(4)}$:

$$E^{(4)} = 2\delta^{(4)}, \tag{69}$$

where $\delta^{(4)}$ is the Kronecker delta with four indices. Hence, as expected, the macroscopic equation in this case (not displayed here) does not have the Navier–Stokes form. Even the linearized equation for sound waves is anisotropic; the waves are damped with a direction-dependent effective viscosity.

On a hexagonal lattice ($M = 6$), $E^{(4)}$ is isotropic, but $E^{(6)}$ is not. Therefore the corrections to the Navier–Stokes equation are anisotropic.

In *three space dimensions* (*3-D*), one can consider vectors $\mathbf{e}_a$ corresponding to the vertices of regular polyhedra (there are only five such). $E^{(4)}$ is isotropic only for the icosahedron ($M = 12$) and the dodecahedron ($M = 20$). Hence a system with icosahedral (dodecahedral) point symmetry would yield an isotropic $E^{(4)}$, but unfortunately it is not possible to fill three-dimensional space with regular icosahedra (dodecahedra).

So one is drawn to the conclusion that no regular lattice in three dimensions (not even a face-centred cubic) can give an isotropic $E^{(4)}$. Only a quasilattice with effective icosahedral or dodecahedral point symmetry can do so. (Remember that we are talking only about models where all the particles have the same speed.)

In *four space dimensions* (*4-D*), there are three regular polytopes which yield an isotropic $E^{(4)}$. These are specified by Schlafli symbols $\{3,4,3\}$, $\{3,3,5\}$ and $\{5,3,3\}$; the items of these lists give respectively the number of edges around each vertex, face and 3-cell. Of these, the $\{3,4,3\}$ polytope yields $E^{(n)}$ that are isotropic upto $n = 4$; it has 24 vertices with coordinates given by permutations of $(\pm 1, \pm 1, 0, 0)$. The other two polytopes yield $E^{(n)}$ that are isotropic upto $n = 8$.

6.9 *Generalizations of results to other models*

We will mention briefly some of the generalizations and results:

(1) Consider a CA model with M unit vectors $\hat{e}_a$ (FHP model has $M=6$). If both $\mathbf{e}_a$ and $-\mathbf{e}_a$ are present and only two-particle collisions are allowed, then one can show that

$$\nu = (M-2)/[2d(d+2)Mf^2(1-f)^{M-3}]. \tag{70}$$

(2) As mentioned before, if in the same basic model we allow more collisions, then the total collision rate will increase, thereby decreasing the viscosity. We have already shown this to be true in the case of model I and its generalizations where all possible collisions are allowed. Similarly, one can show that, for models II and III (which differ only in their collisions),

$$\eta_{\mathrm{II}} > \eta_{\mathrm{III}}. \tag{71}$$

(3) In multiple-speed models, particles with unequal speeds are present, but only a small number of speeds are generally allowed. Some observations about these models are that (a) normally two-particle collisions are sufficient to avoid spurious conservation laws, (b) it is possible to get isotropic hydrodynamic behaviour on cubic lattices, and (c) conservation of kinetic energy is generally violated, but total energy can still be conserved by assigning an internal energy to the particles, for example.

We will discuss the isotropic behaviour in multiple-speed models in some detail. The relevant tensors $E^{(n)}$ in such cases, where particle velocities $\mathbf{e}_a$ with unequal magnitudes are allowed, are

$$E^{(n)}_{i_1 i_2 \ldots i_n} = \sum_a w(|e_a|^2)(\mathbf{e}_a)_{i_1}(\mathbf{e}_a)_{i_2}\cdots(\mathbf{e}_a)_{i_n}, \tag{72}$$

where the $w(|e_a|^2)$ are the weights for different types of particles.

We will consider two examples here. The first one is a model on a square lattice in two dimensions, with the diagonal links also included. In this case, the particle velocities are

$$\mathbf{e}_a = (0, \pm 1), (\pm 1, 0), (\pm 1, \pm 1). \tag{73}$$

Using these in the generalized definition of $E^{(n)}$, one finds that

$$\begin{aligned} &E^{(2)} \text{ is isotropic, and} \\ &E^{(4)} = 4w(2)\Delta^{(4)} + 2[w(1) - 4w(2)]\delta^{(4)}. \end{aligned} \tag{74}$$

The first term, $\Delta^{(4)}$ is isotropic but the second one, $\delta^{(4)}$, is anisotropic. Therefore, for an isotropic $E^{(4)}$, the coefficient of the second term must be zero; that is, we need the condition

$$w(1) = 4w(2). \tag{75}$$

This restricts to four the ratio of the number of particles on the two links.

The second example is a model on a cubic lattice in three dimensions, with the face-diagonal and the body-diagonal links also included. So one has links of three lengths: 1, $\sqrt{2}$ and $\sqrt{3}$. With this model, one gets an isotropic $E^{(2)}$, and $E^{(4)}$ is isotropic

when the condition on the weights

$$w(1)=2w(2)+8w(3) \tag{76}$$

is satisfied.

7. Other issues and concluding remarks

First we will discuss three important issues that merit consideration and which need to be resolved.

7.1 *Thermal effects*

In the FHP model discussed so far, thermal effects are not really present; the local equilibrium is a function of only ρ and $\rho\mathbf{u}$. This is because energy is not independently conserved – it is implied by particle number conservation since all particles have the same speed. This implies that density, temperature and velocity cannot be varied independently, an undesirable feature.

Before proceeding further, we have to first answer the question: What is the temperature in this model? Now, this can be defined in analogy with conventional gases. These have a Maxwell–Boltzmann distribution of velocities $\mathbf{v}$, and the temperature of these gases is defined by

$$(3/2)k_BT=\tfrac{1}{2}[\langle\mathbf{v}^2\rangle-\langle\mathbf{v}\rangle^2]. \tag{77}$$

For the CA models, we therefore use

$$T\sim[\langle\mathbf{e}_a^2\rangle-|\mathbf{u}|^2]\sim 1-|\mathbf{u}|^2 \tag{78}$$

since all particles have the same speed ($|\mathbf{e}_a|=1$). The velocity $\mathbf{u}$ is the hydrodynamic velocity, given by $\langle\mathbf{e}_a\rangle$. This relation implies that the temperature in a region of the CA fluid is completely determined by the local hydrodynamic velocity $\mathbf{u}$.

How do we overcome this problem? One of the ways to have non-trivial thermal effects is to allow for particles with different speeds, i.e., to have a multiple-speed model, so that the energy conservation relation can be independent of particle number conservation. Consider first a *two-speed model*. Let the speeds be c_1 and c_2, and the number of particles with these speeds be N_1 and N_2 respectively. Then it is not difficult to see that

$$T\approx[(c_1N_1+c_2N_2)/(N_1+N_2)]-|\mathbf{u}|^2. \tag{79}$$

However, note that N_1 and N_2 are not independent; they are fixed by the relative weights $w(c_1^2)$ and $w(c_2^2)$ necessary to obtain isotropic fluid behaviour. Also, ρ^{-1} is given by (N_1+N_2). Therefore, T is totally determined by ρ and $\mathbf{u}$.

Let us then consider the next level of complexity, i.e. a *three-speed model*. In this case, we will have

$$T\approx[(c_1N_1+c_2N_2+c_3N_3)/(N_1+N_2+N_3)]-|\mathbf{u}|^2. \tag{80}$$

Here, $\rho^{-1}\approx(N_1+N_2+N_3)$, and isotropy requirements place only one condition on

N_1, N_2, N_3. Thus, in a three-speed model suitably chosen, it is possible to have independent T, ρ, and **u**.

Another possible way to incorporate non-trivial thermal effects is to have models in which the particles carry internal energy. However, much more work has to be done before anything conclusive can be said about either of these possibilities.

7.2 *Models for three dimensions*

It has been noted in the last section that no regular lattice (with only nearest neighbour links) can yield an isotropic $E^{(4)}$. That is, no one-speed-particle model on any regular lattice has sufficient symmetry.

So, it is natural to consider multiple-speed models. One such model was mentioned in the previous section. The model resides on a cubic lattice with links joining sites at distances of 1, $\sqrt{2}$, $\sqrt{3}$; these lengths correspond to the cube edge, face diagonal and body diagonal. The three types of particles have, respectively, speeds of 1, $\sqrt{2}$, $\sqrt{3}$ and velocities given by

$$\mathbf{e}_a = \{(\pm 1, 0, 0)\}, \{(\pm 1, \pm 1, 0)\}, \{(\pm 1, \pm 1, \pm 1)\}. \tag{81}$$

For this model, $E^{(2)}$ is isotropic. But $E^{(4)}$ is isotropic only when

$$w(1) = 2w(2) + 8w(3). \tag{82}$$

This can be achieved by using different collision rules on different time-steps.

Recently two models in three-dimensions have been constructed by d'Humieres *et al* (1986). The first is again a multiple-speed model, but a different one. Here too, the model lives on a cubic lattice, but now the particles have speeds of 0, 1, $\sqrt{2}$. Thus the links which join the sites are the cube edges and the face diagonals, and the model has rest particles as well. Per site, the model can have a maximum of one rest particle, six particles with speeds = 1, and twelve particles with speeds = 2. (Therefore, the model requires 19 bits/site). The condition for an isotropic $E^{(4)}$ is now

$$w(1) = 2w(2). \tag{83}$$

The second one is actually a four-dimensional model but is one lattice-spacing wide in the fourth direction, i.e., it is a three-dimensional slice of a four-dimensional model. In four dimensions, regular lattices with the requisite symmetry exist (d'Humieres *et al* 1986; Wolfram 1986). One of these is the face-centred hypercubic (FCHC) lattice. However, this model is bit intensive; it requires 24 bits/site.

7.3 *Practical limitations on lattice-gas automata*

Are the CA models viable alternatives to conventional methods for high Reynolds number (Re) fluid dynamics? Orszag and Yakhot (1986) answer as follows.

They argue that the computational requirements for CA simulations of continuum fluid dynamics are more severe than for direct simulations of the continuum equations. This they do by comparing the storage (S) and work (W) requirements for CA simulations and direct simulation of incompressible Navier–Stokes equations. Now, it is known that at a Reynolds number Re, the range of excited scales is of order $Re^{3/4}$ and $Re^{1/2}$ in three and two dimensions respectively. This will be the storage

requirement for NS simulations. Also, the computational work (W for NS simulations) required to calculate a significant time in the evolution of large-scale flow structures is of order Re^3 (in three dimensions) and $\mathrm{Re}^{3/2}$ (in two dimensions).

In CA models, the dissipation is modelled through the thermalization of hydrodynamic modes (remember that evolution rules conserve mass, momentum and energy). Therefore the lattice resolution of CA models must be much smaller than that of hydrodynamic simulations, where only scales of the dissipation range or larger need be retained. Thus one has the condition that the CA lattice spacing a must be $\ll$Kolmogorov Scale 1_*. Orszag and Yakhot (1986) give arguments to show that $1_*/a$ increases rapidly with Re. We now present two of them.

(i) This is based on a signal-to-noise ratio argument. In CA simulations, the hydrodynamic velocity $v_H(x)$ at a point x is calculated as

$$v_H(x) = \langle v(x) \rangle, \tag{84}$$

where $v(x)$ is the average (over the cells) CA velocity in a region C_x centred at x, and is given by

$$v(x) = \frac{1}{n} \sum_{i \in C_x} v_i. \tag{85}$$

Here n is the number of occupied sites i within the cell, and the region C_x has linear dimensions $\gg a$. The bracket $\langle \ \rangle$ in (84) stands for space–time filtering, i.e., $v_H(x)$ is calculated by smoothing (filtering) the (noisy) velocity field $v(x)$.

We assume (for simplicity) that the CA particle velocities are given by $v_i = \pm v_{th}$, where v_{th} is the thermal velocity (sound speed) over the CA grid. The condition of low Mach number then implies that

$$v_H \ll v_{th}. \tag{86}$$

Therefore, fluctuations in $v(x)$ are $\sim O(n^{-1/2} v_{th})$.

For a good representation of continuum hydrodynamics, the fluctuations in the velocity v_H must be much smaller than the smallest hydrodynamic velocity, which is the Kolmogorov velocity or the eddy velocity on the dissipation scale 1_*. We denote this velocity by v_*. Thus the condition that noise be small, becomes

$$n^{-1/2} v_{th} < v_*. \tag{87}$$

Note that, in three dimensions,

$$l_* \sim O((\varepsilon/\nu^3)^{-1/4}), \tag{88}$$

$$v_* \sim O((\varepsilon\nu)^{1/4}) \tag{89}$$

where ε is the turbulent energy dissipation rate per unit mass and ν is the kinematic viscosity. Using the above relations, one can see that the number of CA sites n within a region of size 1_* must be

$$n \gg v_{th}^2/(\varepsilon\nu)^{1/2}. \tag{90}$$

But we know that

$$\varepsilon \sim O(U^3/L) \tag{91}$$

where U, L are the macroscale velocity and length; the Reynolds number Re is given by

$$\mathrm{Re} = \mathrm{UL}/\nu, \tag{92}$$

and the Mach number M is

$$\mathrm{M} = U/v_{th}. \tag{93}$$

In terms of Re and M, the condition on n therefore becomes

$$n \gg \mathrm{Re}^{1/2}/\mathrm{M}^2. \tag{94}$$

But we already know that in three dimensions, the range of excited scales, $L/1_*$ goes as $\mathrm{Re}^{3/4}$. Therefore the number n_* of cells of size 1_* within a three-dimensional turbulent eddy of size L scales as

$$n_* \sim \mathrm{Re}^{9/4}. \tag{95}$$

Relations (94) and (95) together imply that the overall number of CA sites (i.e. the storage S) must increase at least as

$$S > \mathrm{Re}^{1/2}\mathrm{M}^{-2}\,\mathrm{Re}^{9/4} \sim \mathrm{Re}^{11/4}/\mathrm{M}^2. \tag{96}$$

To compute W, the work needed, note that the effective evolution time of the fluid system is L/U; this is the turnover time of a large scale eddy. The time step on the CA lattice is a/v_{th}. Therefore, the number of time-steps required for the CA simulation is $Lv_{th}/aU = L/a\mathrm{M}$.

Assuming that the computational work required for each site-update is of $O(1)$, it follows that the total work (W) for the CA simulation is

$$W = (L/a\mathrm{M}) \cdot S = (L/a)(\mathrm{Re}^{11/4}/\mathrm{M}^3). \tag{97}$$

But,

$$(L/a) \sim S^{1/3} (= \mathrm{Re}^{11/12}/\mathrm{M}^{2/3}).$$

This implies that

$$W \sim (\mathrm{Re}/\mathrm{M})^{11/3}. \tag{98}$$

Going through the same arguments in two space dimensions, one gets in two dimensions:

$$S \sim \mathrm{Re}^{3/2}/\mathrm{M}^2, \quad W \sim \mathrm{Re}^{9/4}/\mathrm{M}^4. \tag{99}$$

Expressions (96), (98) and (99) give lower-bound estimates for S and W in three and two dimensions for CA simulations at high Re and low M.

(ii) The second argument is based on upper bound estimates for the Reynolds number. If as before, the discrete velocity v_i of the CA is $\pm v_{th}$ (the sound speed on the CA lattice) and the CA lattice spacing is a, then the kinematic viscosity ν on the CA lattice is at least

$$\nu \geqslant v_{th} a. \tag{100}$$

For self-consistent hydrodynamic simulation, the viscosity ν which is determined on the "molecular" level must equal the viscosity governing the dissipation of hydro-

dynamic modes. Therefore, the Reynolds number of the simulated flow, which is UL/ν, has to obey the inequality

$$\mathrm{Re}\,(=UL/\nu) \leqslant UL/(v_{th}a) \sim ML/a. \tag{101}$$

Now, the total number N of CA sites in the lattice must be

$$N \approx (L/a)^d. \tag{102}$$

Equation (101) then implies that

$$N \geqslant (\mathrm{Re/M})^d. \tag{103}$$

This is nothing but the storage (S) requirement in d-dimensions:

$$S \approx (\mathrm{Re/M})^d. \tag{104}$$

To calculate the computational work requirements, note that as before, the CA simulation of the flow requires at least $L/(a\mathrm{M})$ steps in time. Therefore, the work required is

$$W = S(L/a\mathrm{M}) \approx \mathrm{Re}^{d+1}/\mathrm{M}^{d+2}. \tag{105}$$

Thus, estimates for storage S and work W based on lower bounds for the effective viscosity on the CA lattice are of order

$$S \approx (\mathrm{Re/M})^2, \quad W \approx \mathrm{Re}^3/\mathrm{M}^4, \text{ in 2-D}, \tag{106}$$

$$S \approx (\mathrm{Re/M})^3, \quad W \approx \mathrm{Re}^4/\mathrm{M}^5, \text{ in 3-D}. \tag{107}$$

For easy reference, we present all the above results in tabular form below. The notation used is the following:

NS : conventional simulation of the Navier–Stokes equation;
CA 1 : results of the first argument for CA simulations;
CA 2 : results of the second argument for CA simulations;
Re : Reynolds number;
M : Mach number;
2-D : two dimensions;
3-D : three dimensions.

	Storage S			Work W		
	NS	CA 1	CA 2	NS	CA 1	CA 2
2-D	Re	$\mathrm{Re}^{3/2}/\mathrm{M}^2$	$(\mathrm{Re/M})^2$	$\mathrm{Re}^{3/2}$	$\mathrm{Re}^{9/4}/\mathrm{M}^4$	$\mathrm{Re}^3/\mathrm{M}^4$
3-D	$\mathrm{Re}^{9/4}$	$\mathrm{Re}^{11/4}/\mathrm{M}^2$	$(\mathrm{Re/M})^3$	Re^3	$(\mathrm{Re/M})^{11/3}$	$\mathrm{Re}^4/\mathrm{M}^5$

Therefore if the CA simulations are to have practical utility, then ways have to be found to circumvent these arguments. This is a very important area of research, and merits considerable thought and new ideas.

7.4 *Concluding remarks*

It seems very likely that cellular automaton fluids can serve as a basis for practical hydrodynamic simulations. They are simple to program and are readily amenable to parallel processing. They treat all bits on an equal footing in contrast to floating point representations which treat them hierarchically. Further, the latter lead to numerical instability and require high precision in intermediate calculations. On the other hand, CA models show no unphysical instabilities and are able to handle complex geometries easily.

The macrodynamical equations derived for the CA models in two dimensions, correspond exactly to the Navier–Stokes equation in certain limits. There is qualitative (and quantitative too, for the cases investigated) agreement between theory and simulations in the linear and nonlinear regimes, for moderate Reynolds numbers. The introduction of obstacles into the flow is very simple, and represents a computational overhead of only a few percent. Changes in boundary conditions are also very easy to implement. In conventional simulations of the Navier–Stokes equation, these would imply major changes in the computer programs.

However, a great deal of work has still to be done before one can claim that CA will provide a viable alternative to conventional simulations. No good CA model is available for three-dimensional fluids at the moment. Also, it is not yet clear as to how the CA models fare, as compared to conventional simulations, at high Reynolds numbers which is the region of interest in many situations. Progress in these matters calls for new ideas.

The author would like to thank Prof. R Narasimha for encouragement and several useful discussions, and the Council of Scientific and Industrial Research for financial support.

References

Boon J P, Yip S 1980 *Molecular hydrodynamics* (New York: McGraw Hill)
Broadwell J E 1964 *Phys. Fluids* 7: 1243–1247
d'Humieres D, Lallemand P 1986 *Physica* A140: 326–335
d'Humieres D, Lallemand P 1987 *Complex Systems* 1: 599–632
d'Humieres D, Lallemand P, Frisch U 1986 *Europhys. Lett.* 2: 291 -297
d'Humieres D, Lallemand P, Shimomura T 1985a An experimental study of lattice gas hydrodynamics, Los Alamos Preprint, LA-UR-85-4051
d'Humieres D, Pomeau Y, Lallemand P 1985b *C. R. Acad. Sci. Paris II* 301: 1391–1394
Frisch U, d'Humieres D, Hasslacher B, Lallemand P, Pomeau Y, Rivet J-P 1987 *Complex Systems* 1: 649–707
Frisch U, Hasslacher B, Pomeau Y 1986 *Phys. Rev. Lett.* 56: 1505–1508
Gardner M 1970 *Sci. Am.* 223(4): 120–123
Greenberg J M, Hassard B D, Hastings S P 1978 *Bull. Am. Math. Soc.* 84: 1296–1327
Hardy J, de Pazziz O, Pomeau Y 1976 *Phys. Rev.* A13: 1949–1961
Hardy J, Pomeau Y 1976 *J. Math. Phys.* 13: 1042–1051
Hardy J, Pomeau Y, de Pazzis O 1973 *J. Math. Phys.* 14: 1746–1759
Hayot F, Raj Lakshmi M 1989 *Physica* D40: 415–420
Henon M 1987 *Complex Systems* 1: 763–789
Hillis W D 1984 *Physica* D10: 213–228
Huang K 1965 *Statistical mechanics* (New York: Wiley)

Kawasaki K 1972 in *Phase transitions and critical phenomena* (eds) C Domb, M S Green (New York: Academic Press)
Langer J S 1980 *Rev. Mod. Phys.* 52: 1–28
Manning F B 1977 *IEEE Trans. Comput.* C26: 536–552
Margolus N, Toffoli T, Vichniac G 1986 *Phys. Rev. Lett.* 56: 1694–1696
Nemnich B, Wolfram S 1986 Cellular automaton fluids. 2: Basic phenomenology, Preprint
Orszag S, Yakhot V 1986 *Phys. Rev. Lett.* 56: 1691–1693
Preston K, Duff M J B, Levialdi S, Norgren Ph E, Toriwaki J I 1979 *Proc. IEEE* 67: 826–856
Rivet J P, Frisch U 1986 *C. R. Acad. Sci. Paris II* 302: 267–272
Rosenfeld A 1979 *Picture languages* (New York: Academic Press)
Salem J, Wolfram S 1986 in *Theory and applications of cellular automata* (Singapore: World Scientific) p. 362
Sternberg S R 1980 in *Pattern recognition in practice* (eds) E S Gelesma, L N Kanal (Amsterdam: North Holland)
Sutton C 1981 *New Sci.* 90: 209–211
Toffoli T 1984 *Physica* D10: 195–204
von Neumann J 1963 in *Collected works* (ed) A H Taub (New York: Macmillan) vol. 5, p. 288
von Neumann J 1966 in *Theory of self-reproducing automata* (ed.) A W Burks (Urbana: University of Illinois)
Wolfram S 1983 *Rev. Mod. Phys.* 55: 601–644
Wolfram S 1984 *Physica* D10: 1–35
Wolfram S 1986a *Theory and applications of cellular automata* (Singapore: World Scientific)
Wolfram S 1986b *J. Stat. Phys.* 45: 471–526